High Performance, Low Cost Lateral Metal-Semiconductor-Metal Photodetector for Large Area Indirect X-Ray Imaging

by

Sina Ghanbarzadeh

A thesis
presented to the University of Waterloo
in fulfillment of the
thesis requirement for the degree of
Master of Applied Science
in
Electrical and Computer Engineering

Waterloo, Ontario, Canada, 2013

I hereby declare that I am the sole author of this thesis. This is a true copy of the thesis, including any required final revisions, as accepted by my examiners.

I understand that my thesis may be made electronically available to the public.

Abstract

The most promising technology for radiography is active matrix flat panel imaging systems (AMFPI). However, AMFPI systems are relatively expensive in comparison with conventional computed radiography (CR) systems. Therefore for general radiography applications low cost systems are needed, especially in hospitals and healthcare systems of the developing countries. The focus of this research is the fabrication and characterization of a low cost amorphous silicon metal-semiconductor-metal photodetector as a photosensitive element in a AMFPI systems. Metal-Semiconductor-Metal photodetectors (MSM-PD) are attractive as sensors due to their ease of fabrication and compatibility with thin film transistor fabrication process primarily because there is no p^+ doped layer in comparison with conventional p-i-n photodiodes. We have reported low dark current lateral a-Si MSM-PD (lower than $20pA/mm^2$) with responsivity of $280mA/W$ and EQE of 65 percent to green light ($\lambda = 525nm$). These improvement are achieved by introduction of a PI blocking layer and operating the device at high electric field ($15V/\mu m$). This new structure eliminates the need of p^+ and n^+ layers which makes this structure fully compatible with the a-Si:H TFT fabrication process and consequently a low cost flat panel imager. Further, in this study we have investigated the effect of the spacing and width of the comb structure in the proposed lateral a-Si MSM-PD to determine the best configuration. Moreover, a-Si MSM-PD with PI blocking layer shows a linear behaviour to the photon flux in the wide range of $200nW/cm^2 - 300\mu W/cm^2$ intensity of the incoming light. In comparison to vertical p-i-n structures, the reported MSM lateral device shows gains in terms of dynamic range, ease of fabrication (no p^+ layer) without any deterioration in EQE and responsivity. This results are promising and encourage the development of a-Si lateral MSM-PD for indirect conversion large area medical imaging applications and especially low cost flat panel radiography and computed tomography.

Acknowledgements

I would like to thank all the people who made this possible.

Dedication

This is dedicated to the one I love.

Table of Contents

List of Tables

List of Figures

Chapter 1

Introduction

X-rays have found their place not only in medical imaging, but also in security, industrial and purely scientific purpose since their discovery in 1895 by German Physicist W. K. Roentgen. X-ray discovery opened a new phase in medical diagnosis. X-ray allows us to see things that are invisible to the naked eye and in medicine, it made it possible to diagnose everything from broken bones to breast cancer. For diagnostic purposes, the energy range of incident X-rays to the patient are in the range of $20 - 120 KeV$. Typically, X-ray is categorised by its energy, as shown in table 1.1. Due to the high energy of x-ray photons, the penetration depth is high and is determined by atomic density of the attenuating medium. Therefore, density variation, in the medium can be defined by the x-ray attenuation distribution after exposure.

Table 1.1: X-ray classification and application base on its energy [1]

Application	Energy (keV)	Wavelength ($\mathring{A}$)
Low-energy or soft X-rays	0.1-20	124-0.62
Diagnostic-range X-rays	20-120	0.62-0.1
Orthovoltage X-rays	120-300	0.1-0.04
Intermediate-energy X-rays	300-1000	0.04-0.01
Megavoltage X-rays	$>$ 1MeV	$<$ 0.01

1.1 Conventional Method for X-Ray Imaging

The first medical X-ray image was taken within a month of its discovery [10, 11]. Since then, there have been a tremendous amount of studies on diagnostic X-ray imaging which lead to the development of several methods to capture X-ray images. The first and earliest method was film screening. Film screening is a combination of X-ray film and intensifying screen. Electrons in the x-ray film (which contains silver bromide crystals) are excited and trapped at "Sensitivity centres" in the crystal lattice. In this type of imaging, a dark room and chemical tanks are essential to develop the film. Since absorption of X-rays (in diagnostic range) in X-ray film is only about 2-6 percent, the intensifying screen is coupled to X-ray film to increase absorption efficiency upto 40-60 percent, consequently reducing the amount of x-rays exposed to the patient [12].

Disadvantages attributed to film screening are listed below:

- Limitation of image processing and real time imaging
- Storage difficulties
- Chemical waste problems regarding film development.
- Difficulties in transporting information

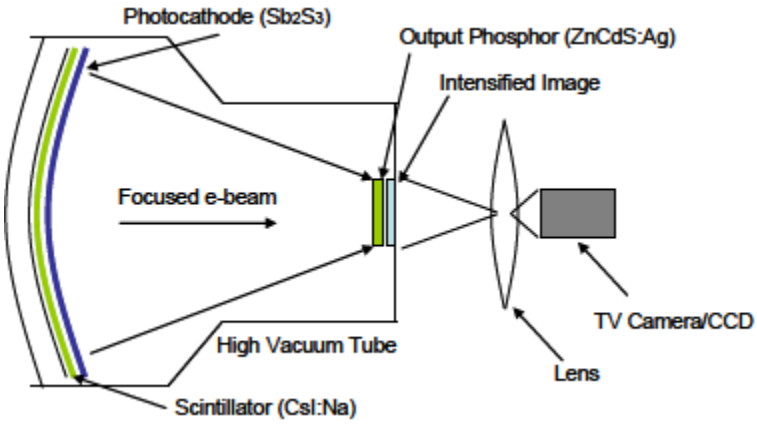

Figure 1.1: Schematic of image intensifier. [3]

In addition to film screening, using image intensifier is another technique to capture an x-ray image. Figure 1.1 shows a schematic of an image intensifier. This method allows real time imaging (fluoroscopic application) by having the capability to be integrated to a charged coupled device (CCD). The image intensifier benefits from a photocathode (such as Sb_2S_3) which converts visible light to electrons. The electrons then accelerate towards the anode in a vacuum tube. The output can be coupled to CCD systems for video monitoring or an optical system directly. However, there are some disadvantages :

- Relatively low image quality
- Expensive maintenance of high voltage (30kV) equipment
- Bulky size of tube
- Considerable manufacturing and maintenance cost

Computed Radiography (CR) is another widely used method of X-ray imaging which has gradually replaced of traditional film screening in hospitals. Equipment used in CR

imaging is very similar to film screening expect that in place of the film to create image, an imaging plate (IP) made of photostimulatable phosphor is used. This method can be used to creat a digital image. The IP stores energy and is scanned by red laser light to develop the image. Therefore computed radiography provides feasibility of image processing to enhance quality of the image.

1.2 Digital Flat Panel Imaging

Digital flat panel X-ray image detectors are the most promising technique for radiography. Ideally, an x-ray imaging system should provide instantaneous and real-time imaging in a digital format with the least amount of exposure as well as reasonable manufacturing and maintenance cost. Conventional X-ray imaging systems, as mentioned, take advantage of photostimulatable phosphor plates (i.e. CR) which prevents any instantaneous and real-time imaging and in order to digitize the image information, scanning by laser system is necessary. Therefore, like traditional film screening, this technique is time consuming and the quality of the image is poor in comparison.
Digital flat panel imaging system are compromised two main components:

1. X-ray detector: Convert X-ray to electrical charge

2. Readout circuit: Store and transfer electrical charge to off-panel circuitry.

Optical imaging systems have a major difference in compared to X-ray imaging. Optical imaging benefits from lenses which project large area field of view on to a device the size of fingernail. On the other hand, x-rays, cannot be focused, so in order to capture x-ray an image of the chest or any other parts of body, an imager with that size is required. Thus,

taking advantage of crystalline silicon technology is limited and tiling would be required to manufacture a large area detector, for example 20cm by 20cm (chest radiography). Conversely, active matrix flat panel imagers (AMFPI) offer great advantage in term of size of the detector. AMFPI uses thin film transistors (TFTs) which are compatible with large are fabrication.

Currently there are two techniques to detect x-rays in flat panel imagers. One is utilizing a photoconductor to convert incident x-ray photons to electrical charge so called as *direct conversion*. The other is *indirect conversion* which benefits from a phosphor layer (also known as scintillator) to convert X-ray to visible light and a photodetector which converts visible light to electrical charge.

1.2.1 Indirect Conversion

Figure 1.2 demonstrates mechanism of indirect detection. Here a phosphor layer (typically $Gd_2S : Tb$ or $CsI : Tl$) is placed in intimate contact with the active matrix array. The phosphor layer converts X-ray photons to light with a specific conversion gain at a certain wavelength (conversion gain is defined as the number of emitted photons per incident X-ray photon). The intensity of light emitted from a particular location of the phosphor is proportional to the intensity of the incident x-ray photons. In order to convert light to electrical charge, each pixel in the active matrix has a photosensitive element (which can be either Schottky M-I-S/M-S-M diode or p-i-n photodiode). The amount of charge determines intensity of light emitted from the phosphor in the region near the pixel. In this type of detection the total conversion gain is a product of scintillator conversion efficiency and the effective quantum efficiency [13]. Hence in order to achieve maximum efficiency, the peak of the emission spectrum of the scintillator should match the absorption spectrum

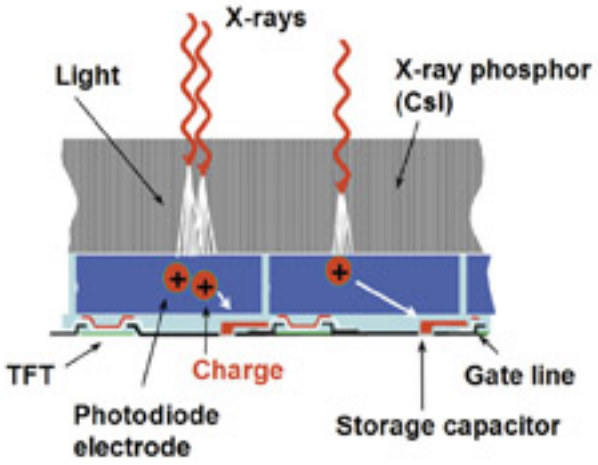

Figure 1.2: Schematic of indirect detection technique. [4]

of the detector.

1.2.2 Direct Conversion

In direct detection, X-ray detection is performed by a thick layer of photoconductor material like amorphous selenium. Thick amorphous silicon, due to its low atomic number (14), is not sufficient for direct detection, even at 1 to 2 mm film thickness . Further, technical difficulties in depositing a stable thick layer of a-Si over a large area has made this material not suitable for direct detection. A cross section of a direction detection detector is shown in figure 1.3 . As it is shown, the thick photoconductor layer is sandwiched between two electrodes. Interacting X-rays produce charge in the photoconductor layer. By applying voltage collection of photogenerated electron/hole occurs. Photogenerated charges are shared between the inherent capacitance of the photoconductor layer and the pixel storage capacitance. The advantage of direct conversion in comparison with indirect

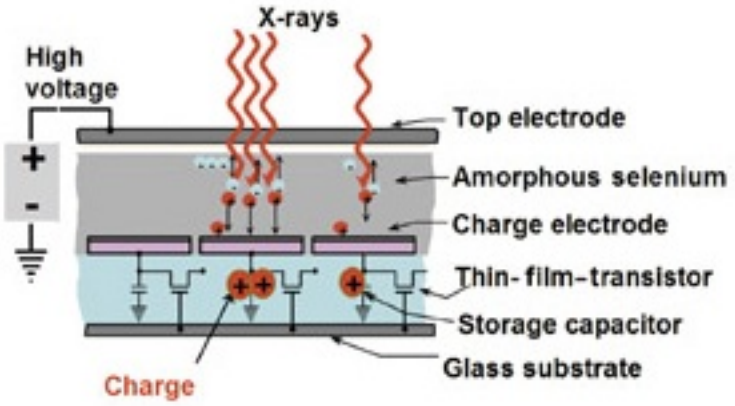

Figure 1.3: Schematic of direct detection technique. [4]

technique is higher resolution and speed due to light scattering of scintillator in indirect detection. However, indirect detection has higher absorption efficiency and consequently, lower dose exposed to patient (for radiography application).

1.3 Low Cost Direct Radiography Imaging

As discussed, the most promising technology for radiography is active matrix flat panel imaging systems (AMFPI). However, AMFPI systems are relatively expensive in comparison with conventional computed radiography (CR) systems. Therefore, for general radiography applications, low cost systems are needed, especially in hospitals and health-care system of developing countries. Different methods have been reported to reduce the cost of existing AMFPI systems. These approachs can be classified into two categories:

- System level modification: targets imaging system cost.
- Device level modification: targets Flat panel imager fabrication cost.

In system level modification, we can consider scanned projection x-ray which was reported by M. J. Yaffe *et al.* [14]. In this technique instead of a two dimensional detector, a one-dimensional image receptor used. The second dimensional is obtained by scanning the x-ray beam and detector across patient. This technique demonstrated an improvement in scattered radiation rejection [14]. Further the cost of the detector is decreased due to the single dimension needed. However, this method requires quite complex and accurate mechanical systems to synchronize scanning of the x-ray tube and the detector. Another method that may reduce cost of the digital radiography system is optically demagnified x-ray screen/camera system. Theoretically, this approach requires a low cost screen and a CCD or even CMOS digital camera. However, coupling x-ray film to a cheap CCD camera without a secondary quantum sink (such as a lens) would result in poor DQE and no significant demagnification [15]. Also introducing a lens raises the cost of the detector and in the best case, quality and cost of the detector would be the same as indirect detection with AMFPI system (which due to the identical size of the screen and flat panel, such that 100 percent optical coupling occurs).

Another approach to lower cost is reducing the cost of flat panel imager itself. Digital flat panel technology initially targeted indirect detection. Active matrix technology that is used in flat panel imagers is the same as standard a-Si:H TFT manufacturing technology used to make displays. One part of AMFPIs that increases the cost is the photosensitive element. Currently most AMFPIs take advantage of p-i-n photodiodes primarily due to their low leakage current, high quantum efficiency. However due to existence of doped p^+ layer, fabrication of photosensitive elements cannot perform with the same process of a-Si:H TFT and it requires separate process which increases final cost of AMFPI. On the other hand, eliminating p^+ layer would increase dark current which is not favourable for detector performance.

1.4 Dark Current Significance

To have an efficient collection process within the photoconductor (direct detection) or photosensitive element of AMFPIs (indirect detection), application of an electrical field is required. By applying an external voltage, photogenerated electrons and holes will flow towards anode and cathode respectively. However, even in absence of x-rays, current will flow through the photodetector, i.e. so-called *dark current*. Dark current of the photodetector determines the lowest amount of x-ray that is detectable by a single pixel of the detector. Thus, having high dark current corresponds to higher exposure of x-rays to the patient in order to be detectable. In addition to shrinking dynamic range of the detector, dark current introduces noise into readout circuity of the AMFPI which increases with the amplitude of the dark current. Typically dark current of photoconductor should not exceed $20pA/mm^2$ [13] especially in integration mode of imaging like computed tomography and general radiography. In fluoroscopy, (real-time imaging) higher dark current is less problematic in comparison with integration mode imaging. In AMFPIs, the photosensitive elements are typically p-i-n photodiodes. Dark current in amorphous silicon stems from two mechanisms. Thermal generation of amorphous silicon and injection of carriers from anode and cathode. Thermal generation of a-Si for a 1mm by 1mm device with thickness of 500nm is approximately 2-3 pA (it will calculate in next chapter). However by applying voltage, the dominant source of dark current is injection of carriers from electrodes. p-i-n photodiodes exhibit great performance because of their high quantum efficiency and low dark current (p and n layers block carrier injection). However, as mentioned earlier, the fabrication of p-i-n photodiodes (due to doped p+ layer) should be performed separately from a-Si:H TFTs, making the detector relatively expensive.

1.5 Objective

The focus of this research is primarily related to the investigation of possibilities to create a low cost indirect conversion digital x-ray imager utilizing amorphous silicon metal-semiconductor-metal (MSM) photodetector as a photosensitive element in a flat panel imager. The criteria considered for the MSM photodetector is performance quality and potential to be manufacturable as a low cost digital radiography system to permit its use for general application, especially in hospitals and healthcare systems in developing countries. In order to lower cost of the x-ray imager, in this work we a propose new structure of a-Si MSM-PD as a replacement for p-i-n photodiode which is commercially used as the photosensitive element in flat panel imagers. The main challenge in this research was finding an approach to minimize dark current without any significant deterioration in its performance through systematic studies on photoresponse of the detector. In this study, in order to achieve the optimum MSM structure having low dark current and comparable quantum efficiency to a p-i-n photodiode, over 100 devices have been produced. The experiments that were carried out to characterize the proposed structure are addressed below:

- Investigation of dark current mechanisms and its stability in proposed a-Si MSM-PD
- Investigation of responsivity and quantum efficiency at different electrical fields.
- Study the effect of fill factor and electrode spacing/width on dark and photocurrent.
- Investigation of detector behaviour under incident power at high and low electrical fields.
- Investigation of temporal response

- Fabrication and study of vertical MSM structure and address challenges

Previously reported a-Si MSM photodetectors exhibit high dark current, dark current instability, low dynamic range and limited EQE to fill factor [16, 8]. Based on results of experiments, we have been able to propose a lateral MSM structure as an alternative to the p-i-n photodiode. These improvement are achieved by introduction of a thin polymer (polyimide) layer as a blocking layer and operating device at high electric field ($15V/\mu m$). This new structure eliminates the need of p+ and n+ layers which makes this structure fully compatible with the a-Si:H TFT fabrication process and consequently a low cost flat panel imager. These results are promising and encourage the development of a-Si lateral MSM devices for indirect conversion large area medical imaging applications, especially for low-cost flat panel radiography and computed tomography.

1.6 Thesis Organization

This chapter has described introductory information on conventional methods for medical imaging, digital flat panel imagers and the importance of low cost x-ray imaging systems. Further, we discussed that in order to bring down the cost of flat panel imagers, a replacement for the p-i-n photodiode as a photosensitive element in flat panel imagers is needed. The next chapter covers brief background information on amorphous silicon and history of the MSM photodetector, followed by fundamentals of a-Si MSM photodetectors including dark current, photocurrent and dynamic range. In chapter 3, the fabrication process of both lateral and vertical structure are briefly described and continues with a brief description of characterization techniques that were used in this work.

Chapter 4 starts with demonstrating improvement of dark current and dark current

stability of the proposed lateral MSM structure without any deterioration in its responsivity. In following, high external quantum efficiency (about 66 percent) is demonstrated and it is discussed that by introducing an anti-reflective layer, EQE can rise up to 80-85 percent. The chapter continues with a study of fill factor and the effect of electrode spacing and width to suggest the best configuration. Further, this chapter covers linearity and non-linearity behaviour of the detector to incident photon flux at high and low electric field. Finally, the detector's temporal response is studied and we demonstrate fall and rise time of 1 ms for $10\mu m$ spacing and width. In chapter 5, the performance (dark and photo response) of the vertical MSM structure is presented and remaining challenges are addressed to improve EQE. Lastly, Chapter 6 concludes this work and summarizes the contributions of this thesis to the field of amorphous silicon technology.

Chapter 2

Background Theory

2.1 Amorphous Silicon Challenges

Amorphous silicon in comparison to crystalline silicon offers some advantages and disadvantages. On the good side, a-Si provides high absorption efficiency within the thin layer (300 - 500 nm), low cost process and large area fabrication which are essential for digital flat panel imagers. On the other hand, due to lack of long range order in amorphous silicon, the density of state concept needs to be revised. However, amorphous silicon retains its short range order because covalent bonds of silicon in a-Si are relatively similar to silicon bonds in crystalline silicon in terms of bond angles, length and number of neighbouring atoms [2]. Since short range order is preserved in a-Si and the energy bond diagram strongly depends on local band configuration [17], with some modifications, DOS of crystalline silicon is applicable to amorphous silicon.

Figure 2.1 illustrates the difference between an atomic network of crystalline silicon and amorphous silicon. Loss of long range order in amorphous silicon results in deviation

of bond length and angle. DOS versus energy of a-Si displays both the conduction and valence band. However, due to deviation in bond length and angle, band tail states inside the forbidden gap are observed. Band tail states are also known as localized states which are spatially confined or trapped [18]. Those states that are located beyond forbidden gap (mobility edge) are known as extended states. Unlike localized states, extended states are not spatially confined. As such carriers in extended states contribute in current conduction. Tail states act as electron or hole trapping centers, based on where they are located within the band gap. Those which are associated to the conduction band act as acceptor states and those which are associated to valence band, act as donor states.

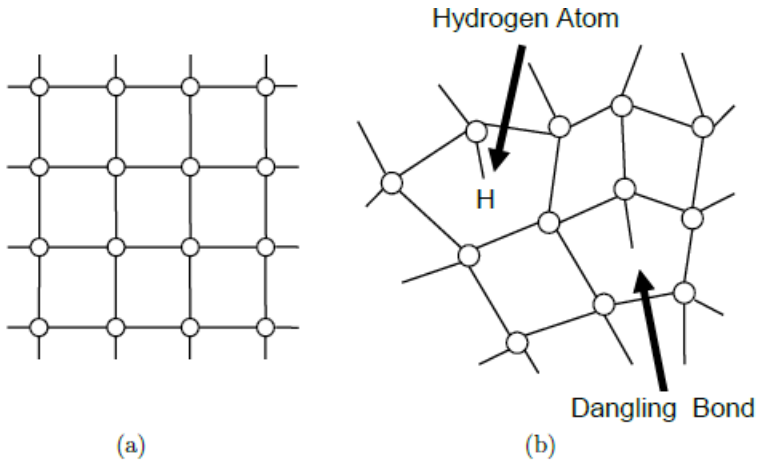

Figure 2.1: Illustration of periodic network of c-Si (a) and random network of a-Si (b). Taken from [5].

In addition to localized tail states, amorphous silicon has deep defect states that are located at mid-gap due to dangling bonds and lattice defects [2]. Dangling bonds result from missing neighbour atoms in quadric bond configuration of Si which leads to the creation of defect states. Figure 2.2 illustrates DOS versus energy in amorphous silicon.

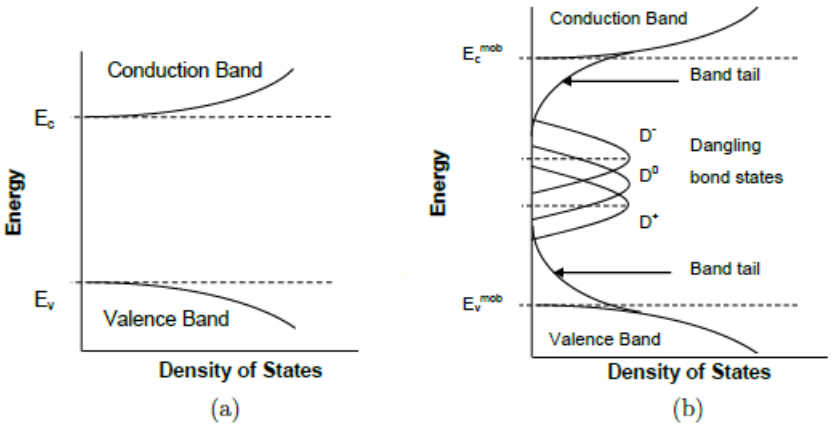

Figure 2.2: Illustration of dansity of state versus energy of c-Si (a) and a-Si (b). Taken from [5].

Deep defect states can act as both electron and hole trapping center (recombination center) and they can be positively and negatively charged [2, 19]. Localized states (mostly tail states) result in instability of dark current in a-Si base MSM photodetectors. In addition to defect states, another challenge of amorphous silicon is light induced degradation, also known as Staebler - Wronski effect [20]. This phenomena was firstly described by Staebler and Wronski in 1977 who state that external excitation of carriers in a-Si causes degradation and creation of defect states due to metastable states in a-Si. It has been shown that light induced degradation is severe in thicker films, hence can be minimized by using thinner films [21]. Alternatively, nanocrystalline silicon can be used instead of amorphous silicon which has not shown degradation under illumination [22]. Table 2.1 presents effect of atomic structure on electronic properties in amorphous silicon [2].

Table 2.1: Atomic structure effects on electronic properties in a-Si [2]

Atomic Structure	Electronic Properties
Bonding Disorder	Band tails, localization, scattering
Structural Defects	Electronic states within the bandgap
Alternative bonding configurations	Metastable states

2.2 History on Metal-Semiconductor-Metal Photodetector

Metal-Semiconductor-Metal photodetector (MSM-PD) are attractive as sensors due to their ease of fabrication and compatibility with thin film transistor fabrication process and/or field-effect-transistors (FETs) in optoelectronic integrated circuits (OEICSs) [23] primarily because there is no p+ doped layer in comparison with conventional p-i-n photodiodes. Moreover, these type of detector would dramatically lower cost and MSM-PDs have demonstrated high operation speed primarily due to low capacitance and consequently lower RC constant time.

MSM structure was first studied at Bell Telephone Laboratories by S. M. Sze *et al.* in 1971 [24]. In 1979, the first MSM photodetector was proposed for high speed optoelectronic circuits, followed by other structures from C. W. Slayman, L. Figueroa and C. J. Wei *et al.* [25, 26, 27]. Between 1988 to 1999, in order to reduce dark current in MSM-PDs, the idea of introducing different passivation layers had obtained much interest among researchers. Sulfured passivation layer for Schottky contacts [28, 29, 30], ultra-thin Au islands [31], introducing SiO_2 layer for InGaAs base MSM-PD [32, 33] and also Polyimide passivation layer [34] have all been studied. Since then, there has been much progress to improve MSM-PD performance in terms of sensitivity, efficiency and speed. The speed of detectors is determined by transient time of photogenerated charge carriers and RC constant time

(charging time) of the external circuit. Typically, transient time of coplanar MSM-PD is less than conventional p-i-n structure due to long travelling distance for carriers in MSM structure in comparison with p-i-n photodiodes. One of the common ways to reduce transient time is shrinking the spacing between electrodes. However, this would increase capacitance of MSM-PD. Therefore there is always a trade-off between these two factors. In literature different MSM structures have been proposed to compromise between transient time and RC time constant [35, 36]. Moreover, there has been some effort to solve the trade-off problem by introducing trench-electrodes Si base MSM [37, 38, 39, 40, 41]. However to fabricate trench electrode reactive ion etching (RIE) is required which makes fabrication complex and expensive due to two stage photolithography. Basically, amorphous silicon MSM structure are favourable for large area medical imaging from an integration point of view and large area fabrication compatibility. Recently a-Si base MSM-PD for indirect large area medical imaging application has been reported [16, 8]. However the earlier devices exhibited high dark current which is problematic for integration mode imaging. In the other words, they were limited in term of dynamic range. Furthermore in the year 2013 Molybdenum disulfide and amorphous silicon heterojunction MSM photodetector has been proposed to improve transient response for fast imaging application such as fluoroscopy imaging [42]

2.3 Fundamental of MSM PD

2.3.1 Dark Current

Charge transport in amorphous silicon is primarily due to two mechanisms, Band-like transport (mobile and extended states) and hopping transport (localized states). Both

mechanisms contribute in reverse current of the Schottky diode. Dark current in Metal-Semiconductor-Metal Schottky diodes stems from four sources: [2, 43, 44, 45, 46]

1. Thermal generation
2. Trapped charges
3. Thermionic emission
4. Tunnelling through junction barrier

MSM photodetectors consist of two back-to-back Schottky diodes. In symmetric MSM photodetectors, metal/semiconductor barrier for both contacts are the same. By applying voltage, one of the diodes will be in reverse mode and the other in forward bias, so most of the voltage would be across the diode which is in reverse mode. Hence, dark current of the MSM structure is determined by reverse current of the Schottky metal/semiconductor contact. The dominant component of dark current is determined by the magnitude of applied voltage [47, 9]. At low voltage (low electrical fields at interface) prevailing sources of current are thermal generation and trapped charges in deep defect states. On the other hand, dominant components of dark current at higher electrical field are tunnelling and thermionic emission (also called thermionic field emission).

In the low voltage case ($E < 2 \times 10^5 V/cm^2$), charge carriers at the conduction band and extended states would sweep away to the output terminal quickly. At this time, the balance between mid-gap states and extended states would be removed. Those mid-gap states which are located below Fermi level are occupied by electrons. After a short time of applying bias and disturbing the equilibrium, electrons in mid-gap states will gain enough energy to reach the conduction band and contribute to dark current. These released charges from mid-gap states would also experience scattering phenomena during travel towards the

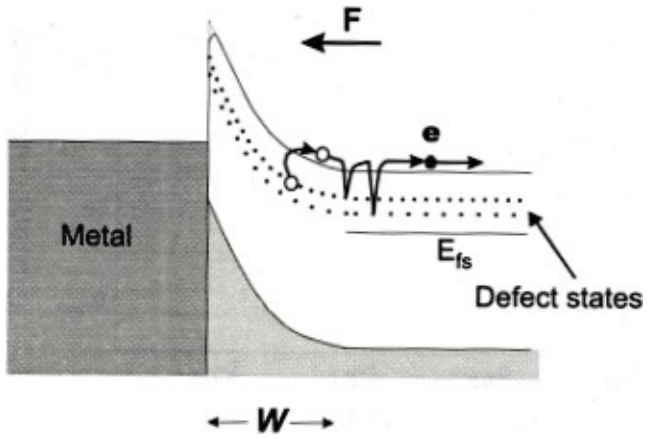

Figure 2.3: Electron transport in a-Si layer; F represents the electric field, Et, shows the Fermi level in a-Si, and w is the depletion width. [6]

junction due to existence of localized states at the band tail of amorphous silicon. Therefore transport of these charge carriers consists of multiple trapping and releasing to reach the output terminal. This type of transport mechanism is called dispersive transport which is fully described by H. Scher *et al.* and T. Tiedje *et al.* [7, 48]

Figure 2.3 describes the basics of dispersive transport mechanism. Briefly, in dispersive transport, sheets of charge carriers in the material would be extended while travelling through the material (due to multiple trapping and releasing) and consequently the output terminal senses current which is varying with time. Figure 2.4 demonstrates typical transient current due to despersive transport [7].

As it can be seen, we have:

$$I \propto t^{-\alpha} \tag{2.1}$$

where α is related to trap state density. Hence, we can say that overall transient behaviour of dark current at low bias (no injection from electrodes) is due to the time needed

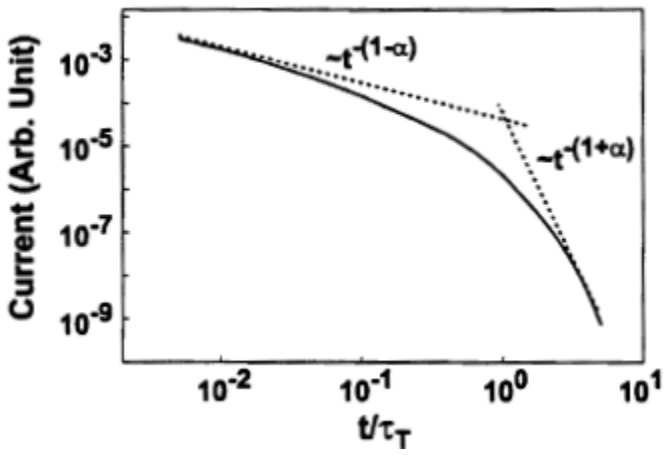

Figure 2.4: Transient current cause by dispersive transient. [6, 7]

to released trapped charges from mid-gap states, plus time it takes to reach the contact terminal due to dispersive transport [47]. Also it's worthwhile to note that dispersive transport would also explain transient behaviour of the Schottky diodes after a short light pulse based on rate of trap filling. We will briefly discuss this in following sections.

At steady state and in absence of injection from contacts, the dominant component of dark current will be thermal generation of a-Si which can be shown as below [2],

$$J_{th} = eN(E_{qF})kT\omega_0 exp[-(E_C - E_{qF})/kT]Ad, \tag{2.2}$$

where $\omega_0 = 10^{13}s^{-1}$ and E_{qF} is quasi fermi level. N is density of trapped states which we take as $N = 10^{17}cm^{-3}eV^{-1}$, where A and d are area and thickness of the film respectively. Also, for intrinsic amorphous silicon we have $E_C - E_{qF} = 0.9eV$ [2] which would result in a current of $\approx 1 - 2pA/mm^2$ for detector with a 400nm i-layer.

By increasing the bias voltage ($E > 2 * 10^5 V/cm$), in addition to thermal generation, thermal field emission and quantum mechanical tunnelling also contribute to dark current. It has been understood that both of these mechanism strongly depend on width and height of the barrier at the metal/semiconductor interface. It has been shown before that the height of the barrier at the metal/amorphous silicon is fairly dependent on the metal work function due to similar densities and energy distribution of surface state at the metal/a-Si interface [49]. However width of the barrier is strongly dependent on electric field and trapped charges at the interface and their release over time. These trapped charges at the interface arise from dangling bonds and defect state in the mid-gap of amorphous silicon [2]. Instability of dark current in amorphous silicon based Schottky diodes has been attributed to release of trapped charge at the interface over time [9]. This implies the fact that the width of the Schottky barrier (which determines rate of tunnelling) changes over time due to release of trapped charges at the interface until it reaches a steady state condition.

As mentioned, before applying voltage, at equilibrium condition, mid-gap states located below Fermi level are occupied by electrons. By applying voltage, mobile carriers in the conduction band and extended states would move towards junction barrier. During the time that it takes trapped charges at mid-gap states to gain enough energy to reach the conduction band, these trapped charges mask the depletion region and bulk of amorphous silicon. Consequently band bending at the metal/a-Si interface would go further than its steady state to bulk of amorphous silicon. Thus, at the moment of applying voltage to the Schottky diode, the width of the barrier at the metal/a-Si would be larger than its steady state, which means a lower chance of quantum mechanical tunnelling through the barrier. As time elapses, those trapped charges which had masked the depletion region would gradually release and reach to conduction band. As a result, depletion width shrinks over time to steady state. Hence, after a few seconds of applying voltage, dark current

tends to increase.

A comprehensive study of reverse current in amorphous silicon based Schottky diode was done by K. Aflatooni *et al.* [9]. According to K. Aflatooni *et al.* total current density of reverse current in a-Si based Schottky diodes is described as:

$$J_{tot} = A^* T^2 exp[-q\frac{(\phi_0 - a||E|| - a||E(t)||)}{kT}], \tag{2.3}$$

where A^* is Richardson's constant, given by,

$$A^* = \frac{4\pi q m^* k^2}{h^3}, \tag{2.4}$$

which is $\approx 120 A/(cm^2 K^2)$ [2]. The tunnelling parameter a depends on effective mass, dielectric constant and etc. T is temperature and E is as electric field which varies in time due to the variation of barrier width at the interface.

Figures 4.3 presents instability of dark current in amorphous silicon base MSM photodetector which were reported before. [9, 8].

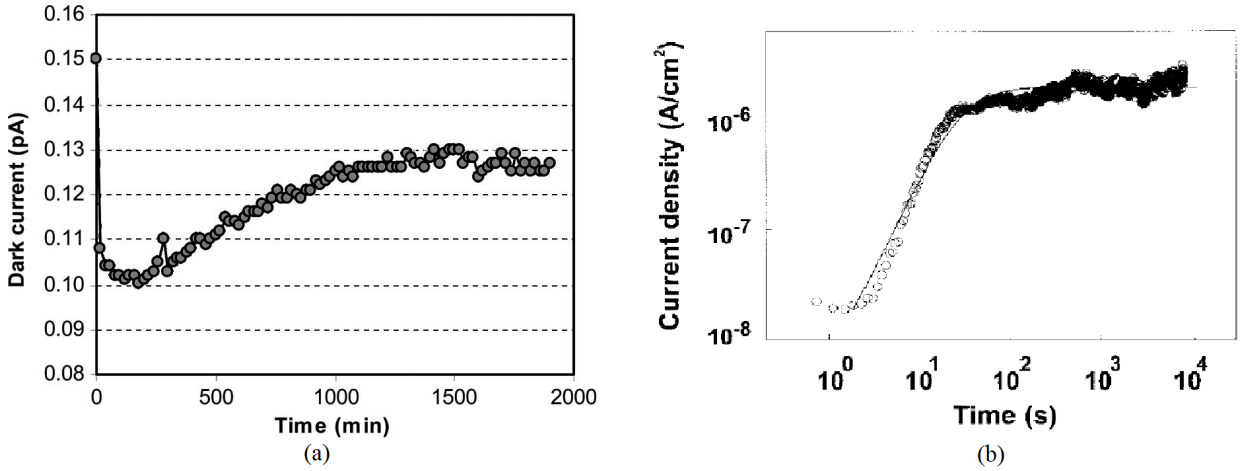

Figure 2.5: Dark current instability under constant voltage over time. Reported by (a) Taghibakhsh *et al.* [8] (b) Aflatooni *et al.* [9].

2.3.2 Photocurrent

Photocurrent in all photodetectors determines the level of responsivity and efficiency of the detector. Photocurrent in steady state arises from different mechanisms including drift, diffusion and recombination of excess carriers. It's been shown that at low electric field, diffusion is the dominant component of photocurrent and by increasing the bias voltage, drift of generated charges would dominant at steady state [50].

By assuming drift is the main component of photocurrent and no space-charge-limited phenomena, we can drive photocurrent in steady state based on optical charge generation [8, 51],

$$J_{ph} = qG_{op}\mu\tau_r E, \tag{2.5}$$

where G_{op} is optical generation, q is charge of electron, E is electric field (which we assumed is constant in between electrode spacing) and $\mu\tau_r$ is mobility-lifetime product which is

dependent on electric field. We should note that due to optical refractive index differences at the interface, some portion of light will reflect at the interface and that the thickness of the active layer determines how much of incoming light will be absorbed. Hence, we can write optical generation as:

$$G_op = (1 - R)(1 - exp(-\alpha t_{a-si}))\frac{P_opt}{h\nu t_{a-Si}}, \tag{2.6}$$

where R is refelectivity, t_{a-Si} is thickness of a-Si, P_opt is power of incoming light and ν is frequency of light. Consequently we would have current of a single MSM PD with gap of L and width of W given as:

$$I_{ph} = q(1 - R)(1 - exp(-\alpha t_{a-si}))\frac{P_{opt}}{h\nu}\mu\tau V\frac{W}{L}. \tag{2.7}$$

It should be noted that we consider infinite surface recombination at the contacts and we neglect the effect of charge diffusion and recombination in the bulk of amorphous silicon. Comprehensive study of photocurrent at steady state in lateral MSM structure by 1D approximation is done by A. W. Sarto *et al.* [50]. However equation (2.7) implies a linear relation between photon flux and photocurrent which is a critical property of photodetectors. We should also consider that by increasing photon flux, we expect to see sub-linear behaviour from the photodetector which can be explained by the effect of the number of incoming photons to mobility-lifetime product [52].

2.3.3 Capacitance

Generally coplanar metal-semiconductor-metal photodetectors are well-known for their low capacitance in compare to vertical p-i-n photodiodes and consequently lower charge and

discharge time during readout [53, 54]. Briefly speaking, as it can be seen in figure 2.6, lateral structure unlike vertical structure consists of two parallel capacitance: one with air (or vacuum) as a dielectric and the other one with amorphous silicon as dielectric. Electrical field in coplanar structure is non-uniform and is more elliptical. It's clear that total capacitance of N electrodes with electrode length and width of l and W respectively and spacing of L would be:

$$C_tot = C_0(N-1)l \tag{2.8}$$

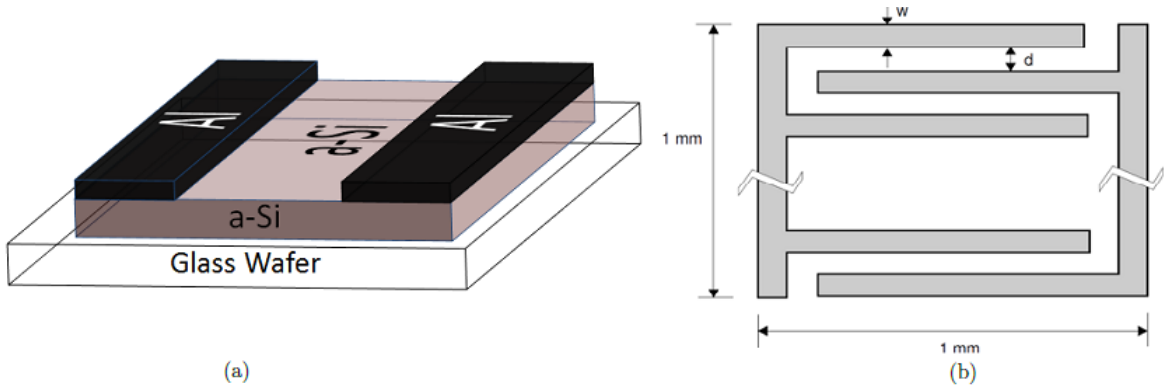

Figure 2.6: Lateral Device structure of MSM-PD, (b) Electrode schematic showing comb structure.

Where C_0 is capacitance of each two electrodes per unit length. As I mentioned, since electrical field is not uniform as it is in vertical structure and it's more like elliptic, we have to use elliptical integrals to drive C_0 [54]. Complete elliptical integral of first kind is defined as:

$$K(k) = \int_0^{\pi/2} \frac{1}{\sqrt{1-k^2\sin^2\phi}} d\phi \tag{2.9}$$

Lim *et al.* [54] has been shown that by assuming infinite thickness of semiconductor,

C_0 is given by

$$C_0 = \epsilon_0(1+\epsilon_s)\frac{K(k)}{K(k`)} \tag{2.10}$$

where

$$k = \tan^2\frac{\pi}{4}\frac{L}{W+L} \tag{2.11}$$

and

$$k` = 1 - k^2 \tag{2.12}$$

2.3.4 Dynamic Range

Dynamic range is one of the most critical factor that determines performance of detectors, specially in medical imaging application where lower dose to the patient is matter of interest. Dynamic rang as detection point of view defines as the range of incoming photon flux that is detectable by detector. It is obvious that dark current of the detector or readout electronic noise determines lower limit of dynamic range. On the other hand, as readout point of view, especially in integration mode , dynamic rang defines as a ability of pixel detector in accumulating charges during integration. Figure 2.7 demonstrate a simple PPS (Passive Pixel Sensor) architecture.

Transistor acts as switch in PPS and charge amplifier is used to read the accumulated at pixel. Output voltage can be given by the following equation:

$$V_{out} = \frac{Q_{ph}}{C_f} \tag{2.13}$$

Thus, maximum signal that we can read in one frame is determined by maximum charge

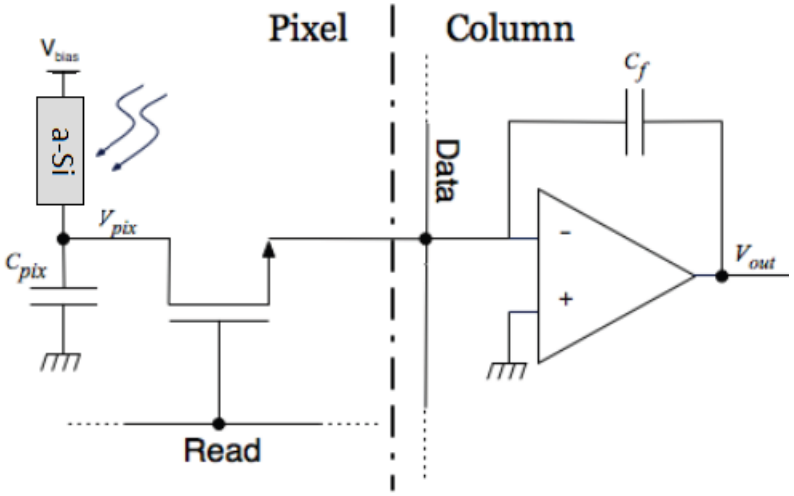

Figure 2.7: Lateral PPS architecture using a-Si detector for digital imaging

that can be accumulated by pixel capacitance. For the maximum charge we have

$$Q_{ph-max} = V_{pix-max}.C_{det} \tag{2.14}$$

$V_{pix-max}$ is determined by working range of detector in term of applied voltage. In conventional p-i-n detector which is widely used in indirect medical imaging, the rang of applied bias to the detector is around $5 - 10V$ (due to breakdown point). By considering the fact that detector should maintain its linearity behaviour in integration mode, the maximum swing of voltage across detector is going to be $250 - 500mV$. Hence, by having a ability to operate detector in high voltage biases, we will improve dynamic range of the detector in integration mode imaging.

Chapter 3

Experimental and Instrumental Methodology

Advantages of amorphous silicon stem from its radiation resistivity, suitability in fabrication and integration with large area flat panels and film uniformity. First, the device structure and process aspects involved with the fabrication of both vertical and lateral a-Si MSM photodetectors are presented in this chapter, followed by various characterization techniques that were used in this research. The fabrication process for lateral and vertical structures takes a 2 and 3 day run respectively based on how the facility operates at that time and the success of each step goes.

3.1 Fabrication Process

Fabrication of the proposed MSM photodetector consists of following process:

- Wafer cleaning and substrate preparation

- Preparation of thin polyimide solution
- Amorphous silicon deposition
- Spin coating of desired polyimide layer (twice for the vertical structure)
- Aluminium magnetron sputtering
- Photo-lithography (required for the lateral structure)

3.1.1 Wafer preparing

High quality deposition of amorphous silicon film requires a clean substrate clear of any contamination such as dust, organic particles, oil, etc. Two different substrates were used in the course of this work: uncoated Corning 7059 type glass (high resistivity) and Corning 1737F glass with one surface coated with a $50nm$ ITO (indium tin oxide) layer for lateral and vertical structure respectively. Regarding the uncoated glass wafer, the cleaning process starts with a typical RCA type 1 to remove organic residue and films. This is followed by ultrasonica bath substrate cleaning with Acetone and Propanol for approximately 5 minutes each. Finally, substrates are dried by using purified Nitrogen gas for about 2 minutes. In the case of ITO coated glass, the cleaning process only includes ultrasonic cleaning with Acetone and Propanol for 15 minutes each and drying.

3.1.2 a-Si deposition

The performance of the proposed MSM photodetector depends strongly on the quality of amorphous silicon which acts as an active layer in the device. The usual method of depositing intrinsic a-Si is by plasma decomposition of Silane gas (SiH_4). Typically, in

absence of plasma, silane decomposes at the temperature of above $450C$ which result in poor quality amorphous silicon film (the high temperature of the substrate prevents hydrogen retention) [2]. An intrinsic a-Si layer for the lateral structure has been deposited using a plasma enhancement chemical vapour deposition (PECVD) cluster tool system. This cluster tool is multi-chambered and has a dedicated chamber for intrinsic a-Si capable of pumping down to $1E-8$ Torr. Substrate temperature is controlled by a heater flush with the substrate and the RF deposition system is capacitively coupled parallel plate RF ($13.56MHz$). During deposition, the substrate faces down in the chamber. Amorphous silicon was deposited at $250C$ using pure SiH_4 (no hydrogen dilution).

Due to limitations with the PECVD cluster tool, we weren't able to deposit the i-layer for the vertical structure with the same system and recipe that we used for the lateral structure. As mentioned, in the PECVD cluster tool, during deposition the substrate is facing down. In the lateral structure, since the substrate is uncoated corning glass, this won't cause a problem. However, for the vertical structure -where a-Si is sandwiched between two thin polyimide layers- the substrate is ITO coated glass with cured polyimide coated on it. Since the deposition is happening at $250C$, by putting the ITO substrate with polyimide inside the PECVD cluster tool chamber, the risk of polyimide peeling off to the chamber is high. In courtesy of other lab users and to avoid contamination, I switched to a single chamber Plasma Therm VII PECVD system (Substrate faces up in this machine).

3.1.3 Thin Polyimide

Polyimide is a well-known insulator in CMOS fabrication. Recently, there has been several studies on polyimide conduction mechanisms at high electric field [conduction PI] as well as using polyimide as a blocking layer to prevent injection of carriers into the active layer

[13]. Polyimide is available commercially in both sheets (needs only curing process) and solution (needs spin coating and curing process). In this research we have used polyimide in solvent. $1\mu m$ polyimide is reported as a blocking layer for a-Se MSM structures [13]. Since resistivity and thickness of the proposed a-Si base MSM-PD is lower than the previously reported a-Se MSM-PD, polyimide films with a thickness of equal or less than $300nm$ was needed. The least viscose polyimide solution that is available commercially is PI 2610 from HD-MicroSystems. The coating process for this type of polyimide is spin coating and the thickness of the film is determined by RPM. As it is mentioned in PI 2610 data sheet, the thickness of the film is going to saturate at at $5000rpm$ which leads to a minimum thickness of $800nm - 1\mu m$. In order to spin coat thin polyimide, I dilute the solution with adhesion promoter T-9038 with equal volume weight. Some points should be considered during the making of a thin polyimide solution, otherwise film quality after spin coating and curing would be likely poor.

- Polyimide should be kept inside freezer (between -10 to -18C) and before using it, it is necessary to wait untill solution temperature reaches room temperature otherwise humanity will diffuse into polyimide. Moisture contamination is detrimental to polyimide stability and must be avoided based on datasheet.

- First certain amount of polyimide (i.e $3 - 6ml$) should be poured into clean bottle (preferably no syringe used), followed by adding known amount of adhesion promoter (T-9038) (i.e $3 - 6ml$).

- In order to mix the solution, any kind of quick movement should be avoided to prevent creation bubbles inside the solution. It is recommended to turn bottle rotated very gently for about 3-4 minutes.

- The thinned solution should be allowed to age 12 hours at room temperature (20 C, 70 F) before use. This time is needed for the solution to reach equilibrium condition.

To coat around $150 \pm 25nm$ polyimide, spin coating at speed of 5 krpm is needed for 30 sec. Table 3.1 shows spin coating steps and condition.

Table 3.1: PI spin coating process steps

	Duration(sec)	Speed (rpm)	Acceleration (rpm/sec)
Step 1	7	500	250
Step 2	35	5000	1000

After spin coating, in order to vaporize the solvent we carry out two prebaking steps and one curing step which are described in tables 3.2 and 3.3 respectively.

Table 3.2: Pre-baking process

	Duration(sec)	Temperature (C)
Step 1	90	90
Step 2	90	150

Table 3.3: Curing process

Duration(hr)	Temperature (C)	Ramp (C/hr)
2	350	240

3.1.4 Electrodes

In both the lateral and vertical structure, the last step of fabrication is sputtering and patterning electrodes. Aluminium has been chosen as a metal electrode. In the vertical case, since the area of a single pixel device is big ($1mm^2$), no photo-lithography is needed

and pattering can be done by using shadow masks. In the lateral structure, patterning electrodes is an unavoidable step. MA6 was used for the lithography step. Different device configurations have been designed to understand performance of the detector.

3.1.5 Device Structure

Both lateral and vertical structure are fabricated using a $1mm^2$ square exposure area. As it was shown before, the lateral structure consists of a comb structure of electrodes (fingers) with varying width and spacing. Three different configuration have been fabricated including:

- Width of $10\mu m$, Spacing $15\mu m$,
- Width of $10\mu m$, Spacing $10\mu m$,
- Width of $5\mu m$, Spacing $10\mu m$,

which results in fill factors of 60, 50, 66 percent, respectively. Figure 3.2(c) shows the 1mm by 1mm device that consists of 40 individual lateral devices with width of $10\mu m$ and spacing of $15\mu m$. The device structure of the vertical s-Si MSM photodetector is also shown in figure 3.1.

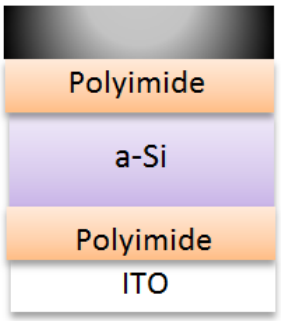

Figure 3.1: Cross section of vertical structure.

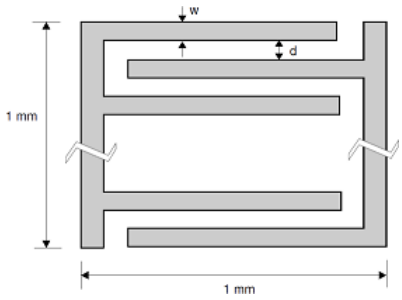

(a)

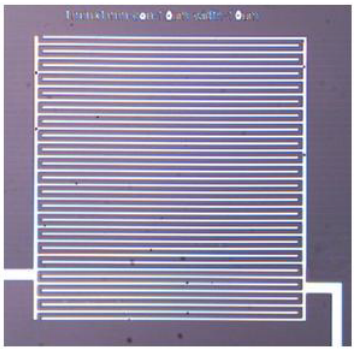

(b)

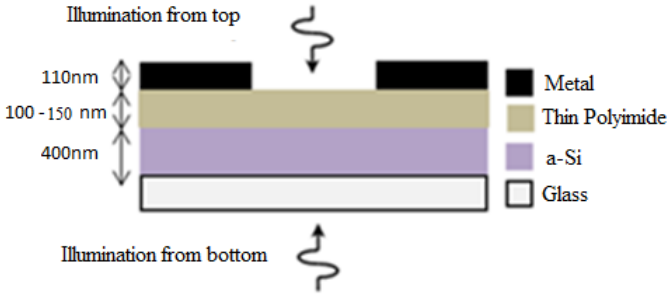

(c)

Figure 3.2: (a) Lateral a-Si device layout structure (comb structure), (b) Micrograph of the fabricated detector, and (c) Cross section schematic of a-Si MSM with blocking layer.

3.2 Characterization Techniques

MSM photodetector performance is characterized by dark current, dark current stability, external quantum efficiency, responsitivity, linearity to incident photon flux and temporal response. In this work, dark current and photoresponse was recorded by an Agilent Semiconductor Parameter Analyser (4156C) and low-noise micro-probe station. Regarding biasing the device, a Stanford Research Systems PS350 high-voltage power supply was used. Illumination happened from the bottom and top with a monochromatic LED (green, blue and red). Intensity of incident light was also measured using a Newport 1935-R optical power meter. Also MEDICI (Synopsis Inc.) was used to simulate and estimate the electric field within the a-Si layer. Since the Agilent Semiconductor Parameter Analyser is too slow for transient measurements, another set-up was used to record the transient response of the detector. The measurement set-up that was used for temporal response of the device is described in figure 3.3 which consists of a Ametek 5182 low-noise current to voltage amplifier and fast digital oscilloscope.

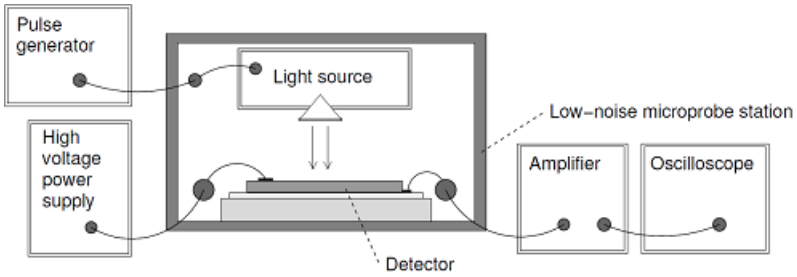

Figure 3.3: Experimental set-up for time response measurment.

Chapter 4

Lateral Amorphous Silicon Based MSM Photodetector

4.1 Introduction

Amorphous silicon metal-semiconductor-metal photodetectors are attractive as a photosensitive element in indirect X-ray detection due to their compatibility with large area a-Si thin film transistors (primarily because there is no p+ doped layer, unlike conventional p-i-n photodiodes). Recently an a-Si based MSM photoconductor for medical imaging applications has been proposed [16, 8]. However these devices exhibited high dark current which is problematic for integration mode imaging. In the other words, they were limited in terms of dynamic range. Further, previous studies of dark current on a-Si based MSM-PD found dark current instability [8, 9]. In this study we demonstrate an a-Si MSM lateral structure with significantly low dark current (high sensitivity),high responsivity, high dynamic range and reasonable speed.

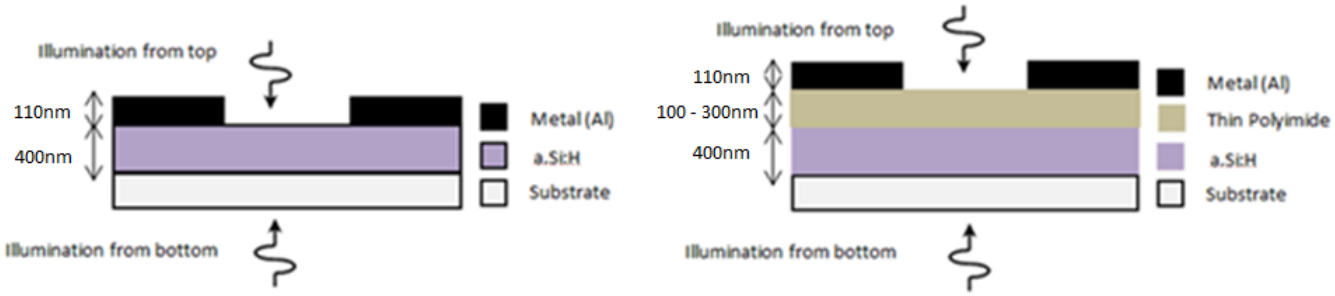

Figure 4.1: Lateral MSM a-Si:H device structure (left) and lateral MSM a.Si:H with blocking layer (right). As you can see we have both option of lighting from top and bottom. Thin PI can be considered transparent for green light.

In this chapter, as a base line, performance of a simple in house fabricated a-Si MSM structure (figure 4.1 left) was investigated in terms of dark current, photoresponse and responsivity. This structure is similar to previously studied a-Si MSM-PD [16, 8]. This is followed by a comprehensive characterization and development of a high performance MSM lateral structure with low and stable dark current. The improvements of the proposed structure in terms of dark current and stability are achieved by the introduction of a thin polymer layer as a blocking layer. Figure 4.1 demonstrates two lateral MSM structures.

4.2 Lateral a-Si MSM (without blocking layer)

4.2.1 Dark Current and its instability

In this section the performance of the a-Si MSM lateral photodetector (without blocking layer) is going to be investigated. As mentioned in the second chapter, MSM photodetectors consist of two back to back Schottky diodes and since the proposed structure is symmetric, by applying voltage results in one being in reverse mode and the other in forward mode.

Therefore, dark current of MSM-PD is controlled by reverse current of the a-Si Schottky diode. It is understood that dark current in MSM diodes stems from two mechanisms: thermionic emission and tunnelling (at medium bias voltage range). Both strongly depend on width and height of the barrier at metal/semiconductor interface. It has been shown before that the height of the barrier at the metal/amorphous Si is fairly dependent on the metal work function due to similar densities and energy distribution of surface states at the metal/a-Si interface for different metals [49]. This implies that by increasing the voltage across MSM-PD, a dramatic increase in dark current is expected since at medium rage electric field ($> 2 \times 10^5 V/cm$), dark current is controlled by quantum mechanical tunnelling which is highly dependent to the field at barrier rather than thermal generation which is fairly field dependent. As shown in figure 4.2 , dark current is highly dependent on voltage bias which leads to high dark current under favourable condition, consequently reducing dynamic range and sensitivity. It should be noted that for medical imaging application due to the desire to reduce the amount of x-ray exposure to patient, dark current shouldn't exceed $20pA/mm^2$ in indirect conversion technique [13] [shiva lateral] primarily due to noise and dynamic range.

In addition to the significantly high dark current of a-Si based MSM-PDs, instability of dark current is a well-known problem for these typess of Schottky diode base detector. Figure 4.3 demonstrates previously reported dark current instability in amorphous silicon MSM structure [8, 9]]. I have observed the same issue with our in-house fabricated a-Si MSM photodetector as shown in figure 4.4.

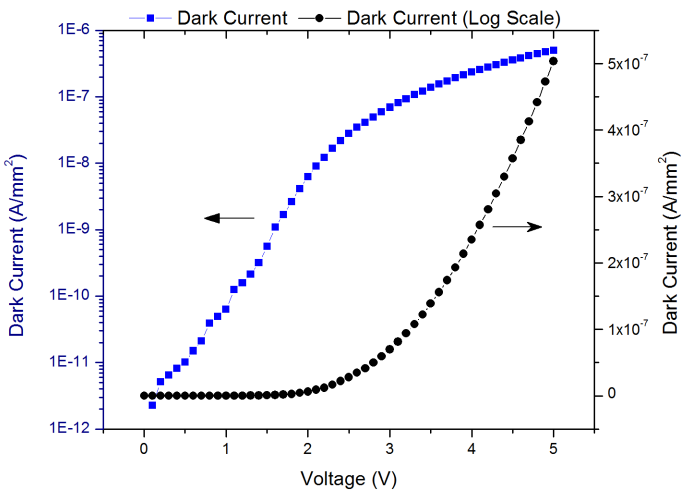

Figure 4.2: Dark current versus voltage for MSM detector without blocking layer.

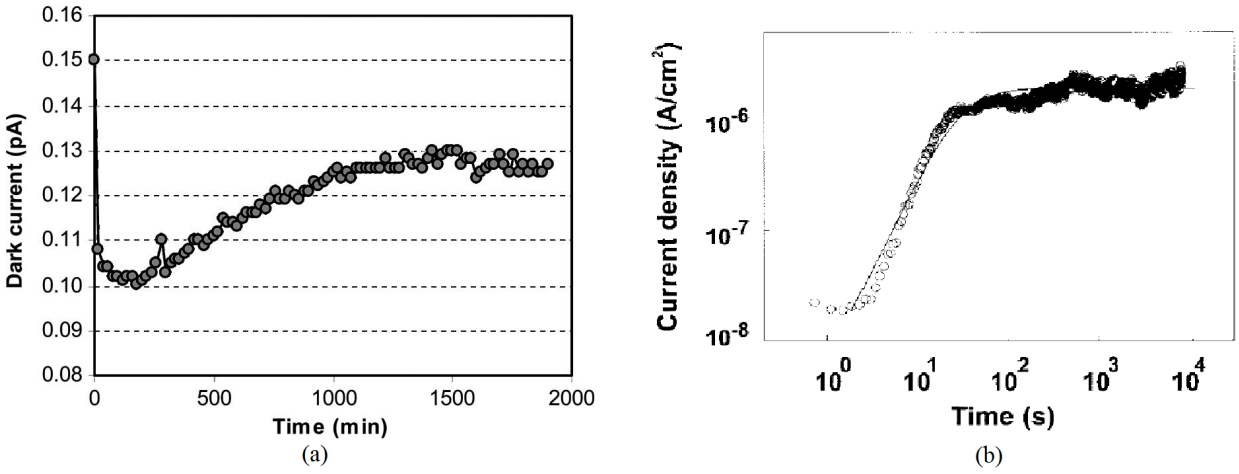

Figure 4.3: Dark current instability under constant voltage over time. Reported by (a) Taghibakhsh *et al.* (b) Aflatooni *et al.*.

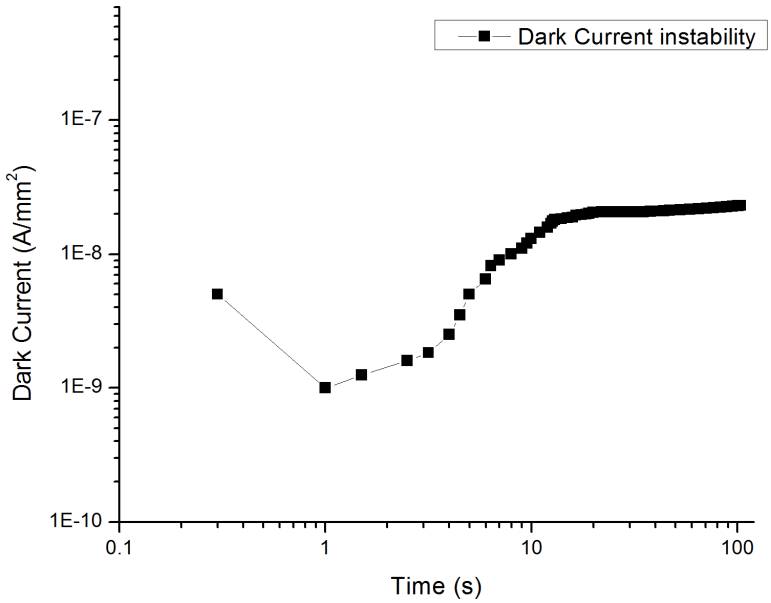

Figure 4.4: Dark current instability of in house fabricated MSM-PD under constant voltage of $2.5V$. .

4.2.2 Photoresponse

Photoresponse determines responsivity, sensitivity and efficiency of the detector. As mentioned in second chapter, by assuming no space charge limited phenomena, we can simplify photocurrent based on incoming power density and applied voltage,

$$I_{ph} = q(1-R)(1-exp(-\alpha t_{a-si}))\frac{P_{opt}}{h\nu}\mu\tau V\frac{W}{L}. \tag{4.1}$$

Figure 4.5 demonstrates the response of the in-house fabricated a-Si MSM-PD (with width and spacing of 10μ) to green light ($\lambda = 525nm$) at an intensity of $73.2\mu W/cm^2$ as a function of applied voltage. As it can be seen, the photoresponse is nearly linear as a function of applied voltage in this range of incoming photon flux . It should be noted that by increasing photon flux, sub-linear behaviour is expected from detector due to the dependence of mobility- lifetime product to photon flux [52].

Furthermore, figure 4.6 demonstrates sensitivity (I_{on}/I_{off}) of in-house fabricated a-Si MSM which has a dramatic drop with voltage (from 5×10^3 to 10^1) due to injection of carriers from the Al/a-Si contact at higher voltages, consequently increasing dark current. Hence, from a sensitivity point of view, and in order to maintain low dark current ($20pA/mm^2$) the operating range of a-Si MSM-PDs is confined to ($0.5-1V$).

In integration mode imaging like Computed Tomography (CT), due to the charge accumulation at pixel capacitor, voltage across detector varies over time. Since the a-Si MSM-PD operating range is around $0.5-1V$ and the response is strongly dependent on applied voltage, a small variation of voltage across detector (and consequently a change in electric field) leads to non linear behaviour, adding noise to whole system. This issue in addition to the dark current problem limits the use of a-Si MSM-PD in indirect detection mode of medical imaging (as an alternative to p-i-n photodiode).

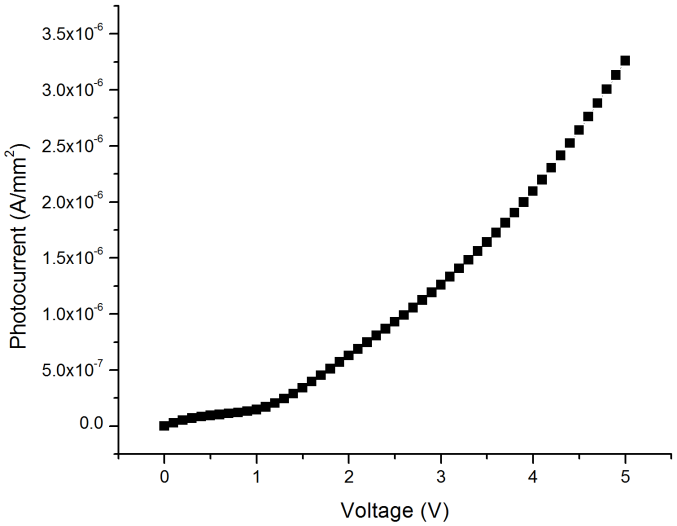

Figure 4.5: Photocurrent density versus voltage of the in-house fabricated a-Si MSM with width and spacing of 10μ to green light with $73.2\mu W/cm^2$ intensity.

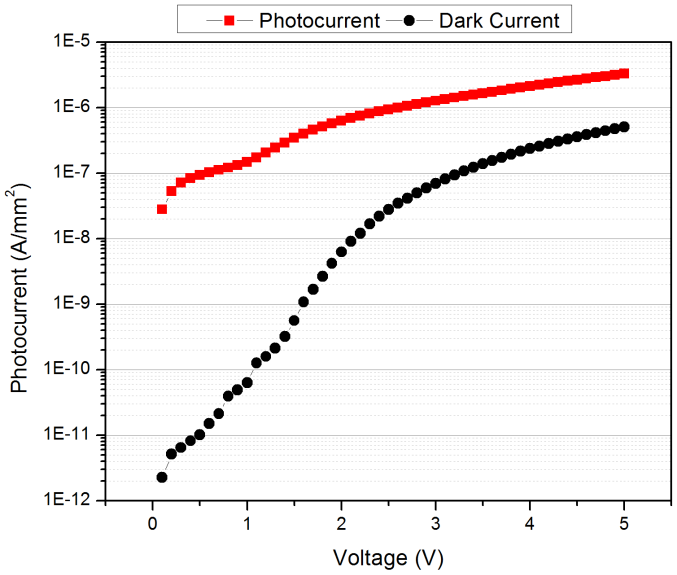

Figure 4.6: Dark and Photoresponse at different voltages for a-Si MSM-PD. Width and spacing of 10μ Incoming light: green light with $73.2\mu W/cm^2$ intensity.

4.3 Introducing the Blocking layer

The advantages of utilizing a-Si MSM photodetectors for medical imaging have been stated (large are fabrication, low cost, compatibility with TFT fabrication process, high responsivity and reasonable operation speed) in comparison with conventional p-i-n photodiodes. On the other hand, according to the characterization of the lateral a-Si MSM photodetector (without blocking layer) in section 4.2, it can be concluded that lateral a-Si MSM detectors are problematic in integration mode due to high dark current and its instability. In addition to the dark current issue, as we discussed earlier, the operating range of a-Si MSM-PD is $0.5 - 1V$ which limits the dynamic range from a readout point of view and adds noise to the system by small variations in voltage. Therefore, we propose a new a-Si lateral MSM photodetector ,with a polymer blocking layer, to overcome these problems. In this section the operation of the lateral a-Si MSM structure with the blocking layer is investigated. Also, as discussed in the third chapter, different lateral MSM structures with different spacing and width were fabricated, but the active area for all designs are the same ($1mm^2$). In this thesis the comb structure with spacing and width of $15\mu m$ and $10\mu m$ respectively has been selected as a main structure due to the highest fill factor among fabricated detectors (details in following sections).

4.3.1 Dark Current and its stability

The improvements of the proposed structure in terms of dark current and stability are achieved by the introduction of the thin polymer (Polyimide) layer as a blocking layer which prevents injection of carriers into the amorphous silicon. Figure 4.7 demonstrates dark current as a function of applied voltage. We have reported dark current before and after illumination to show whether the detector would recover after illumination. Dark

current before illumination was recorded 100 seconds after applying the voltage, and dark current after illumination was recorded 60 seconds the after pulse light. Figure 4.8 shows a timing diagram for the experiment.

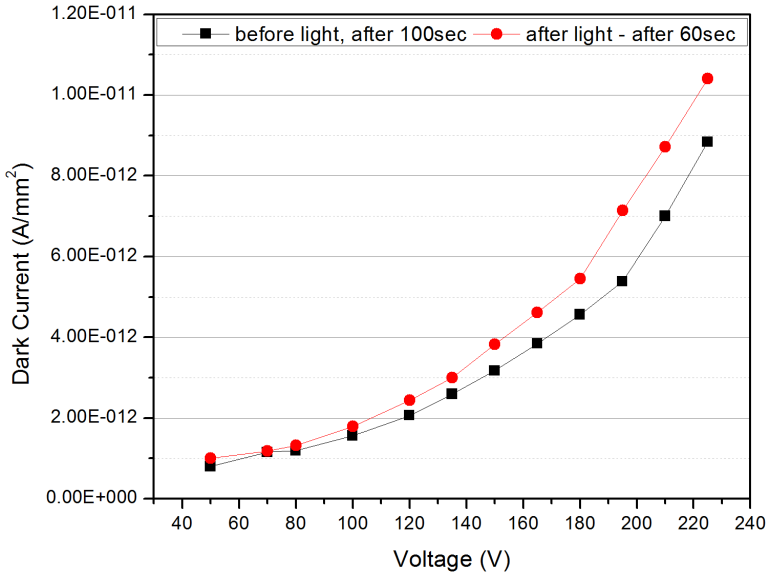

Figure 4.7: Darkcurrent (before and after illumination) as a function of applied voltage for a-Si MSM-PD with PI. Width and spacing of 10μ and 15μ respectively.

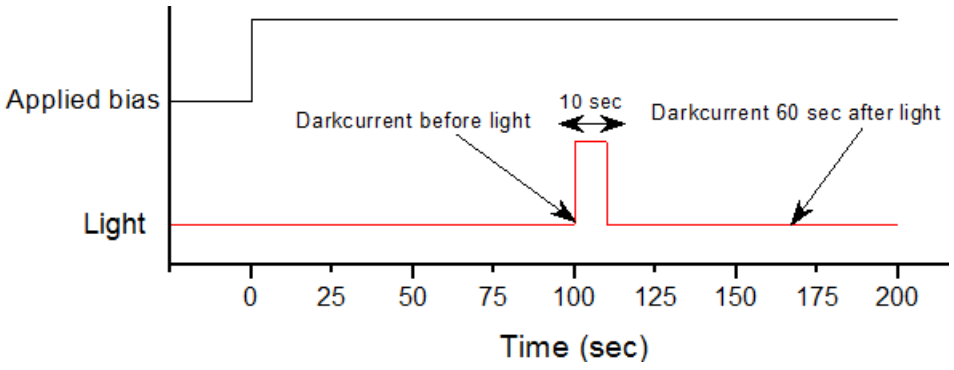

Figure 4.8: Time diagram of darkcurrent measurment.

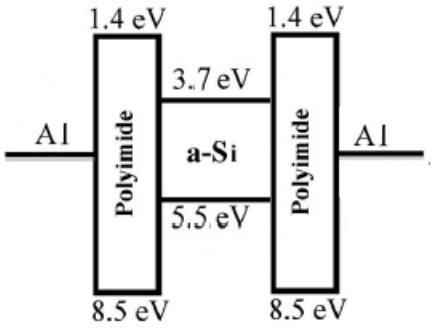

Figure 4.9: Energy level schematic for the a-Si MSM with blocking layer investigated in this study.

As seen in figure 4.7, dark current is in range of amorphous silicon thermal generation which is calculated in second chapter. This implies that polyimide acts as a blocking layer and reduces the tunnelling probability of carriers from aluminium to amorphous silicon. This can be understood by examining the energy level diagram of Al/PI/a-Si which is shown in figure 4.9 . Polyimide is typically used as an insulator layer in CMOS process and it's a well-known insulator because of its wide band gap.

Regarding dark current stability, unlike previously reported a-Si MSM detectors [16, 8, 9], the proposed a-Si MSM detector with the PI layer as a blocking layer hasn't exhibited any instability issues. As shown in figure 4.10, we experimentally demonstrated that by applying a thin Polyimide layer between metal and amorphous Si, the stability of dark current improves primarily due to increasing the barrier and reducing the chance of tunnelling. It has been shown that dark current instability in a-Si Schottky diodes results from releasing trapped charge over time at the interface of metal/amorphous Si, consequently reducing the width of barrier and increasing tunnelling rate through barrier [9]. This only applies to medium range electric fields where the prevailing source of dark current is tunnelling and thermionic field emission, both of which depend highly on width

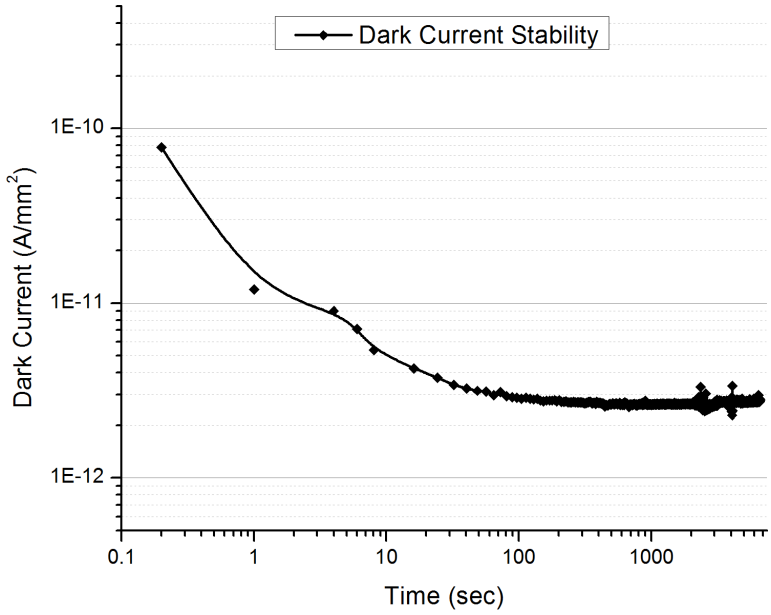

Figure 4.10: Dark current stability of lateral MSM detector with Polyimide Biased at 150V.

and hight of the barrier. In the proposed structure, due to the existence of the blocking layer, the dominant mechanism of dark current is thermal generation (even at medium and high fields) and consequently, variation of the barrier width does not effect transient behaviour of dark current. Figure 4.10 indicates dark current over time at $150V$ bias voltage.

4.3.2 Photoresponse

We have demonstrated that by introducing a thin PI layer in between metals and amorphous silicon, dark current and its stability in lateral MSM-PD are improved. These improvements would be beneficial if the photoresponse is not curtailed by the polyimide layer. The photodetector is illuminated from the bottom (through the glass wafer) with

green light ($\lambda = 525nm$) at an intensity of $9.5\mu W/cm^2$. Figure 4.11 shows the photoresponse as a function of applied voltage. Photocurrent was record after $10sec$ of continuous illumination.

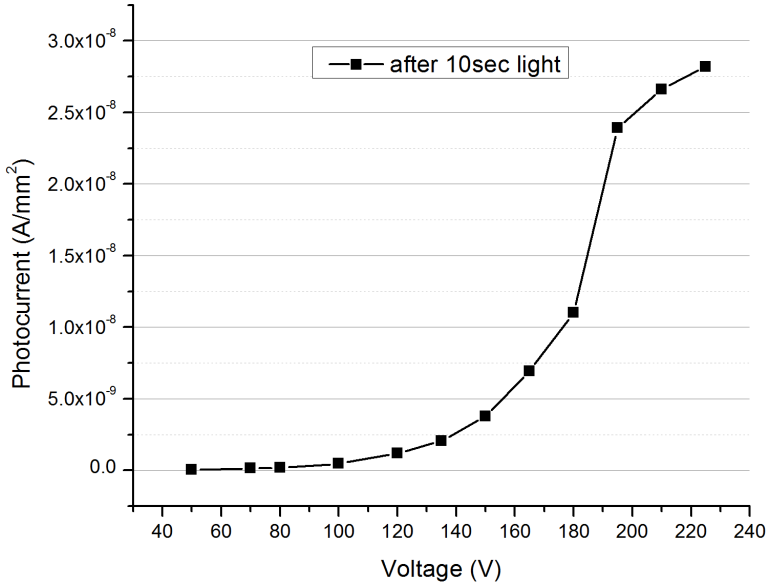

Figure 4.11: Photocurrent density versus voltage of in-house fabricated a-Si MSM with the PI blocking layer exposed to green light ($\lambda = 525nm$) with $9.5\mu W/cm^2$ intensity

As shown in figure 4.11, unlike what is was mentioned before in equation 4.1, for the a-Si MSM lateral detector with blocking layer, photocurrent doesn't appear to have a linear behaviour to voltage. In order to understand the current behaviour in proposed MSM-PD and how polyimide layer conducts under light, it is essential to investigate the conduction mechanism inside polyimide and other layers in dark and photo mode. Figure 4.12 demonstrates conduction path in a single lateral MSM structure with PI (path for electrons is the reverse). As shown, no charge would travel along PI to reach other electrode (charge carriers always choose path with lowest resistance). At steady state and in absence of light,

the resistance of channel (active layer)(R_2) is high and comparable with resistance of PI (R_1 and R_3), so the bias voltage would be shared between these three resistors. However, once illuminated, due to charge generation inside amorphous silicon, the resistance of the channel would decrease dramatically. Thus, most of the bias voltage would drop across the polyimide layer (R_1 and R_3). Conduction in polyimide films at high electric field has been investigated comprehensively by N. R. Tu *et al.* [55]. They demonstrate that at high-field ($> 1.4MV/cm$) polyimide film starts to conduct due to Fowler-Nordheim type tunnelling injection of electrons [55]. Hence, decreasing resistivity of the channel leads to drop around $150 - 200$ Volt across $200nm$ PI (around $7.5 - 10MV/cm$) and consequently, conduction would be happen through PI. Moreover, in order to verify whether charge is going through PI and no charge is accumulated at PI/amorphous silicon interface during illumination, a pulse modulation measurement has been conducted which will be discussed in upcoming sections.

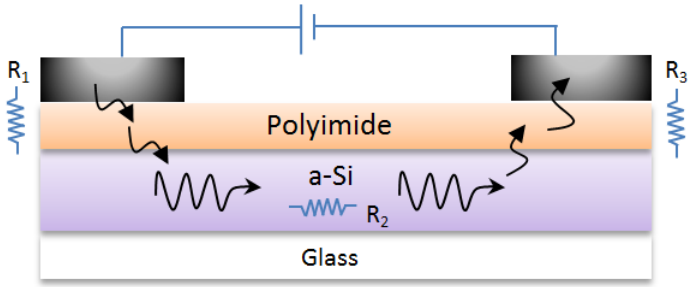

Figure 4.12: Conduction path of the proposed a-Si MSM photodetector with PI blocking layer. R_1 and R_3 are the resistance of $100nm$ PI, R_2 is resistance of channel which varies based on incident light

Another point that is noticeable in figure 4.11, is the fact that after $200V(13.3V/\mu m)$ the photocurrent tends to saturate. As I mentioned before, the operating range of the detector should be ideally independent of small variations in voltage, especially in integration mode

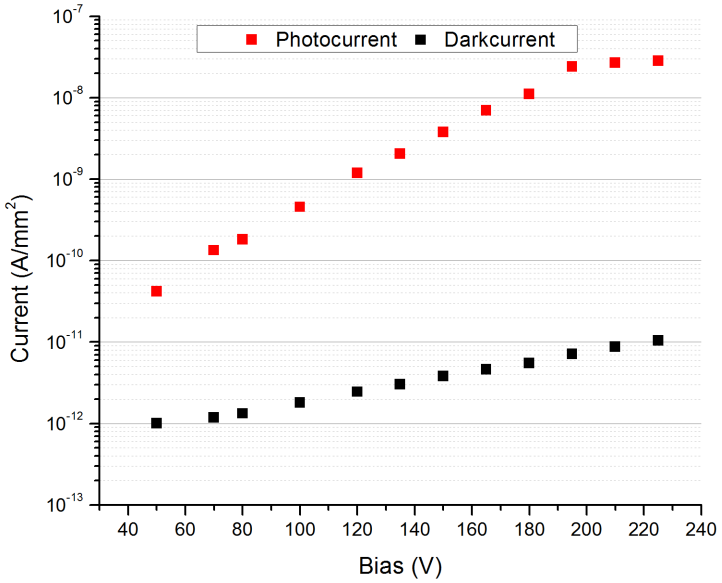

Figure 4.13: Photocurrent and dark current as a function of voltage. Dark current was recorded 60sec after illumination. Incident light: Green ($\lambda = 525nm$) at intensity of $9.5\mu W/cm^2$

imaging. Therefore, the proposed a-Si MSM photodetector exhibits remarkable dynamic range from a readout point of view (capable of operating in high voltage) while it maintain dark current as low as $15pA/mm^2$. Furthermore, figure 4.13 demonstrates sensitivity (I_{on}/I_{off}) of the proposed a-Si MSM with PI which indicates significant sensitivity (2×10^3) to low levels of light ($9.5\mu W/cm^2$).

4.3.3 Responsivity and EQE

In addition to dark current, external quantum efficiency (EQE) and responsivity are other performance metrics of interest. A detector's EQE indicates the capability of the detector in terms of charge generation and charge collection and photresponsivity defines electro-optic transfer gain. Both these parameters depend on photocurrent and optical power of

incident light. EQE and photoresponsivity are respectively given as,

$$EQE = \frac{(I_{ph} - I_{dark})}{P_{inc}\lambda}\frac{hc}{qn}, \tag{4.2}$$

$$PR = \frac{I_{ph}}{P_{inc}}, \tag{4.3}$$

where P_{inc} is incident optical power equal to $I_{inc} \times A$ (I_{inc} is intensity of light and A is area of the device), q is electrical charge of electron, h is Planck's constant, λ is wavelength of incident light, c is speed of light and n is index of fraction of air. Therefore we would have $\frac{hc}{qn} = 1.2395 \times 10^3 W.nm.A^{-1}$.

Figure 4.14(a) and 4.14(b) show EQE and responsivity of the a-Si MSM-PD with PI as a function of applied voltage. As can be seen, above $200V$ we are reaching saturation which results in an EQE of $60-65$ percent. It should be taken into account that due to the difference in index of fraction of incident light in air, glass and amorphous silicon some portion of light cannot reach amorphous silicon surface. In order to calculate the portion of reflected light, the surface reflectivity is used equation(4.4).

$$R = \frac{(n_1 - n_2)^2}{(n_1 + n_2)^2}, \tag{4.4}$$

where n_1 n_2 are the refractive indexes of source and destination, respectively. Since before the a-Si surface, we have two interfaces, the total reflectance (R_{tot}) is $R_1 + R_2(1-R_1)$. Also the refractive index of air, glass and a-Si at $\lambda = 525nm$ is $1, 1.52$ and 4.44. Thus, total reflectance of green light would be around 0.25. This implies that by utilizing a proper anti-reflective back plane, EQE can reach to $80-90$ percent. Regarding responsitivity, our proposed a-Si MSM structure with PI has shown great responsivity (around $280mA/W$)

which is higher than previously reported a-Si MSM photodetectors [8, 42].

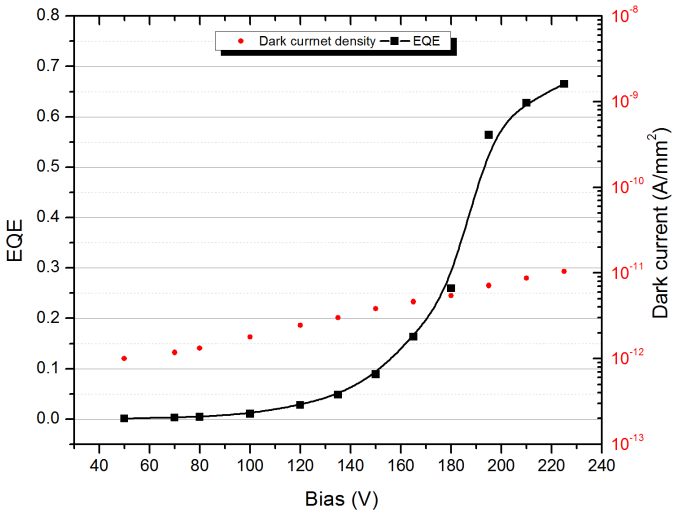

(a) EQE as a function of voltage

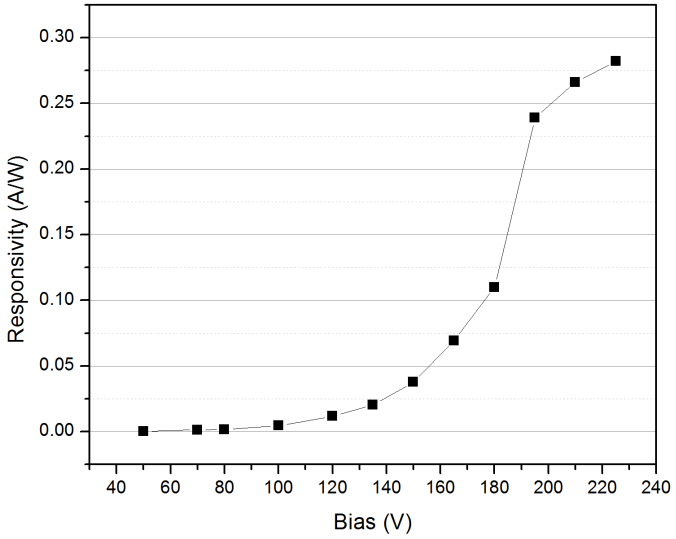

(b) Responsitivity as a function of voltage

Figure 4.14: EQE and responsivity of the in-house fabricated a-Si MSM with PI blocking layer. Incident light: Green ($\lambda = 525nm$) at intensity of $10\mu W/cm^2$

4.3.4 Pulse modulation

In section 4.3.2 we claimed that photogenerated charge carriers tunnel through polyimide at high electrical field. For further verification, a pulse modulation measurement has been conducted. In this measurement, the device was rested at a given voltage for 30 minutes and then was exposed to four light pulses.

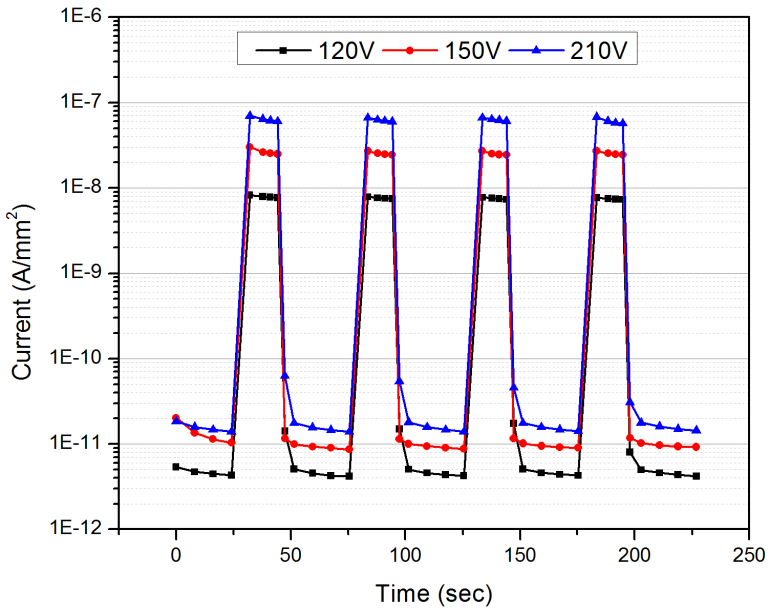

Figure 4.15: Pulse modulation photoresponse of lateral MSM detector with Polyimide. Incident light: Green ($\lambda = 525nm$) at intensity of $9.5\mu W/cm^2$. Pulse period = $50sec$ and Width = $20sec$

Tunnelling of charge carriers through polyimide implies that no charge will be accumulated at PI/a-Si interface. Accumulation of charge carriers at the interface results in an internal electrical field against external electric field (field that is due to applied voltage) which will reduce photocurrent in sunsequent pulses. Therefore, no photocurrent reduction is expected during pulse modulation. Figure 4.15 demonstrates no photocurrent reduction, consistent with our prediction.

4.3.5 Linearity to Photon Flux

In addition to dark current and photoresponse, linear behaviour of the detector to incident photon flux is important from a readout point of view. As discussed earlier, photocurrent should have linear behaviour with the intensity of incident light (equation 4.1). However, it is expected to observe sub-linear behaviour at high photon flux. Two mechanisms might attribute to this phenomena :

- Absorption and/or photogeneration saturation within $400nm$ a-Si by increasing number of incident photons
- Collection efficiency degradation due to the dependence of mobility-lifetime product on incident photon flux [52]

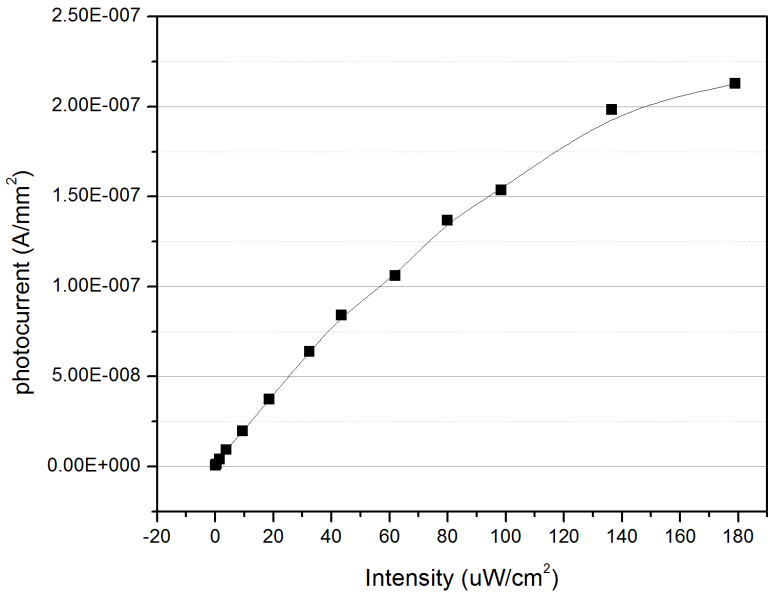

Figure 4.16: Photoresponse versus photon flux at $150V$ voltage

Figure 4.16 exhibits linearity of photocurrent to the intensity of incident light ($\lambda = 525nm$) at $150V$ applied voltage. Sub-linear behaviour is observed at high intensity as we mentioned earlier. In order to understand which mechanism is dominant in the sub-linear region, we have to determine the sub-linear behaviour at higher electric field (higher applied voltage). If the response tends to decay at lower intensity at lower electric field, this would imply that sub-linear behaviour is a result of collection efficiency reduction at higher intensity because of the dependence of mobility-lifetime product on the number of incident photons. Figure 4.17 shows normalized responsitivity as a function of incident intensity for two different applied voltages, $150V$ and $210V$. We observed significant decay of responsivity at higher intensity for $150V$ applied voltage which indicates that th prevailing mechanism in the sub-linear behaviour is the dependence of mobility-lifetime product and consequently loss of collection efficiency at higher intensity. Furthermore, figure 4.18 shows the response of the detector as a function of incident light intensity at 210V applied voltage and represents wide detection dynamic range (from $200nW/cm^2 - 300\mu W/cm^2$).

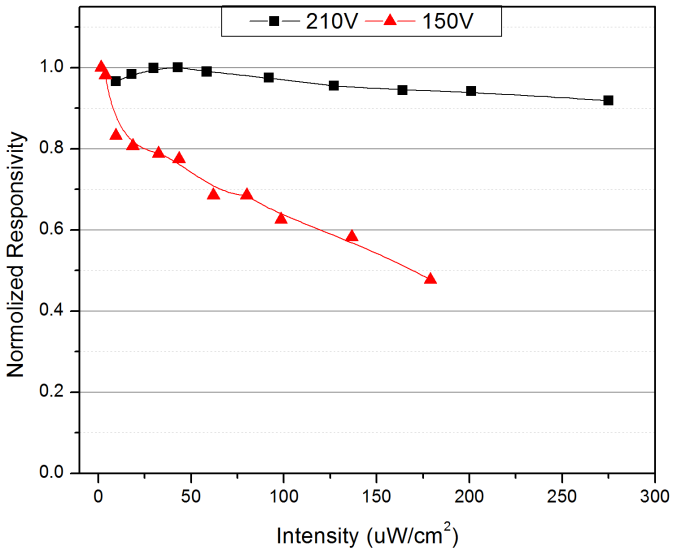

Figure 4.17: Normalized responsivity as a function of intensity at $150V$ and $210V$ applied voltage

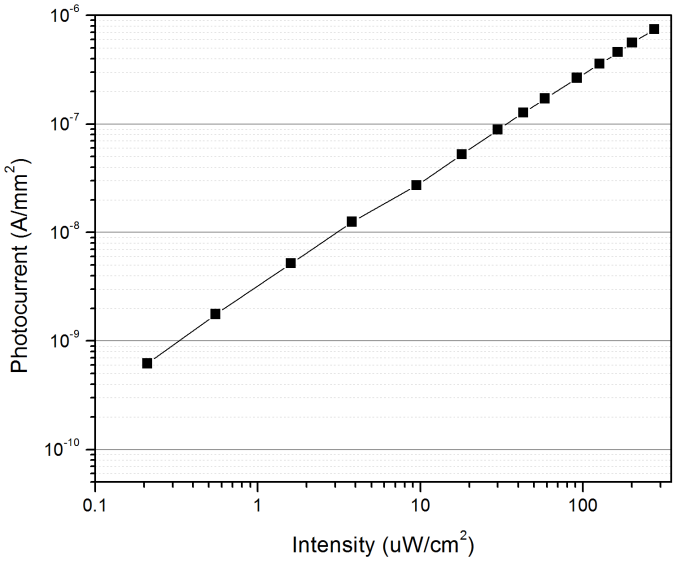

Figure 4.18: Photocurrent as a function of intensity at $210V$ bias. This result demonstrates high detection dynamic rage. Light source: Green ($\lambda = 525nm$)

4.3.6 Effect of Electrode Width and Spacing

Our proposed a-Si MSM photodetector consists of a comb structure of electrodes (fingers) with a varying comb width and spacing as shown in figure 4.19 . Utilizing this structure would result in a fill factor less than one. Fill factor is defined as active area of the device (where absorption and collection occurs) over total area of the device. In the comb structure with a spacing of s and a width of w, fill factor would be:

$$FF = \frac{s}{s+w} \tag{4.5}$$

In case of top electrode structure (like our proposed PD) with spacing and width of $15\mu m$ and $10\mu m$, respectively , top illumination would result in a fill factor of 60 percent due to masking light by electrodes and no absorption below electrodes. However, in bottom illumination, photons are absorbed by amorphous silicon below electrodes, but it is expected that due to lack of electrical field below electrodes, collection is expected to dropped dramatically in the electrode-covered area [8, 56]. Figure 4.20(b) demonstrates

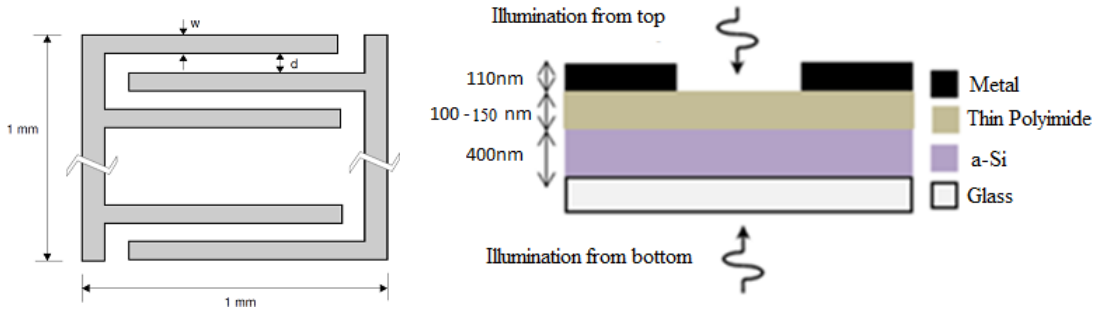

(a) (b)

Figure 4.19: (a) Lateral a-Si device layout structure (comb structure), (b) Cross section schematic of a-Si MSM with PI blocking layer.

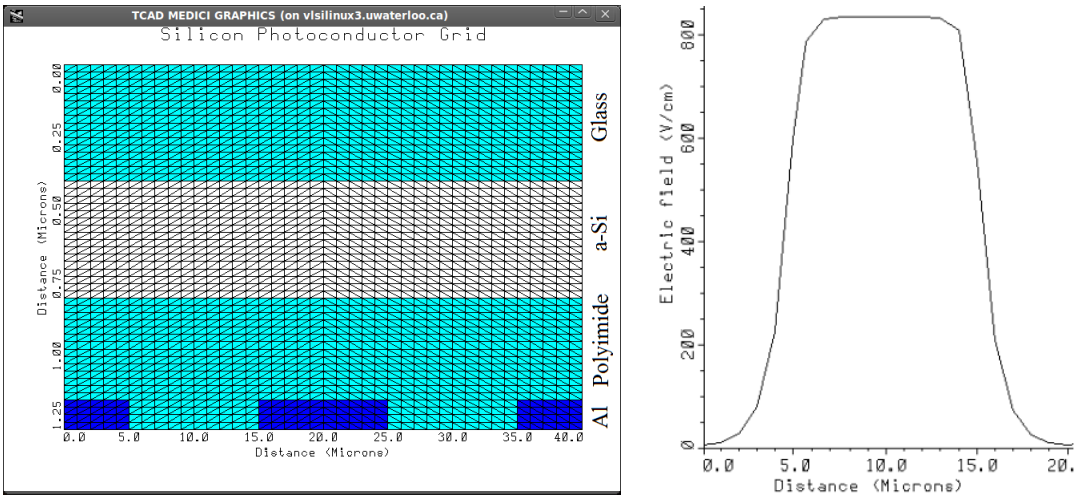

(a) (b)

Figure 4.20: (a) Cross section of simulated device structure (width and spacing of $10\mu m$ (b) Electrical field distribution in amorphous silicon layer in a single device

2D simulated results for the distribution of electric field as function of distance from electrodes. The simulation has been carried out by TAURUS MEDICI and the structure of the simulated device is shown in figure 4.20(b) (width and spacing of $10\mu m$ was chosen). Figure 4.20(a) shows the non-uniformity of the electric field in the active layer, which implies that poor collection efficiency is expected below the electrodes in comparison to within the electrodes, due to lack of electric field.

Therefore, by shrinking the electrode width, we expect higher fill factor and consequently higher quantum efficiency. Figure 4.21 shows photo and dark current of two in-house fabricated a-Si MSM-PD, one with spacing and width of $10\mu m$ (Sample 1) and the other one has spacing and width of $10\mu m$ and $5\mu m$ respectively (Sample 2). As expected, the photocurrent ratio between these two device is around 1.3 which is ratio of their fill factor (66 percent over 50 percent). On the other hand, we observed different behaviour

in dark current. Although the spacing of the electrodes are the same in both structures, higher dark current is observed for sample 2 at the same bias voltage. Also after $130V$, there is a dramatic increase in dark current in sample 2 which could be attributed to pin holes inside polyimide due to high electrical field at edge of Al electrode and PI. In order to understand the behaviour of dark current with respect to variation of electrode width, we simulated the electric field distribution in polyimide layer. Figure 4.22 shows the electric field distribution in the polyimide layer and at the interface of the PI/Al contact in sample 1. As can be seen, at the edge of the electrode, the electric field has a peak which means that the chance of tunnelling and pin holes is high. This implies that by shrinking the electrode width, fill factor is increased, but on the other hand we are increasing electric field at edge of electrode and PI (even at same voltage), consequently increasing dark current. Thus, shrinking width of electrode too much, forces us to the operate detector at lower voltage to maintain dark current in a favourable range, consequently losing photocurrent and quantum efficiency.

In section 4.3.3, we observed EQE as high as 66 percent within lateral device with width and spacing of $10\mu m$ and $15\mu m$ respectively. We should consider the fact that around 25 percent of incident photons will be reflected at the glass/air and amorphous silicon/glass interface. Therefore internal quantum efficiency (defined as a number of collected charges over a number of absorbed photons) of 80-90 percent is achievable. There are two possibilities that may lead to higher internal quantum efficiency than fill factor, including having photo-gain inside a-Si or having collection below electrodes (where electric field is lower than within electrodes). In order to verify which mechanism occurs, photodetector is illuminated from top. In this case, since electrodes mask the incident light, no absorption and collection happen bellow electrodes. It should be noted that in the top illumination case, there are air/PI and PI/a-Si interfaces which results in 33 percent reflectance of light

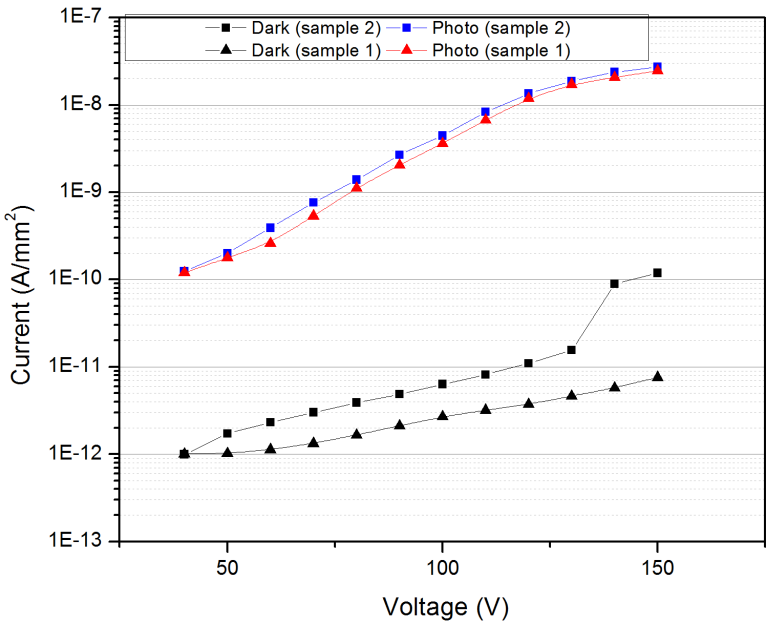

Figure 4.21: Photo and darkcurrent of sample 1 (spacing and width of $10\mu m$) and sample 2 (spacing and width of $10\mu m$ and $5\mu m$ respectively. Light source: Green $\lambda = 525nm$ at intensity of $9.5\mu W/cm^2$)

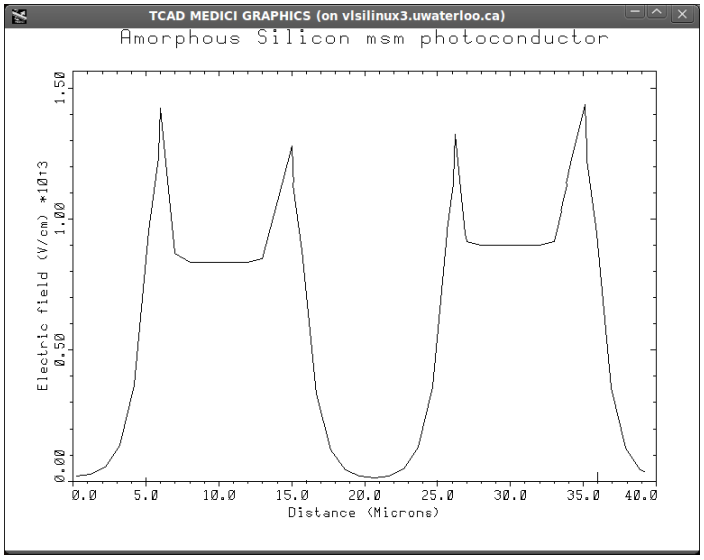

Figure 4.22: Electrical filed distribution in Polyimide - sample 1 (spacing and width of $10\mu m$)

(100nm of PI transmit 90 percent of light at $\lambda = 525nm$ [13]). In this measurement, the device with a spacing and width of $10\mu m$ (50 percent fill factor) at $120V$ was tested. Figure 4.23 illustrates the response of the detector to green light ($\lambda = 525nm$) at intensity of $10\mu W/cm^2$ in top and bottom illumination case.

In order to perform a valid comparison and consider reflectivity of light at the interfaces, we calculated internal quantum efficiency (IQE) for top and bottom illumination. IQE is defined as the number of collected electrons over total number of absorbed photons. Since the thickness of a-Si in the structure is 400nm, we can assume all photons which reach surface of active layer will be absorbed. IQE is given as:

$$IQE = \frac{I_{ph} - I_{dark}}{P_{inc}(1-R)\lambda}\frac{h.c}{q.n}, \tag{4.6}$$

where R is reflectivity at the interface which is approximately 0.33 and 0.25 for top

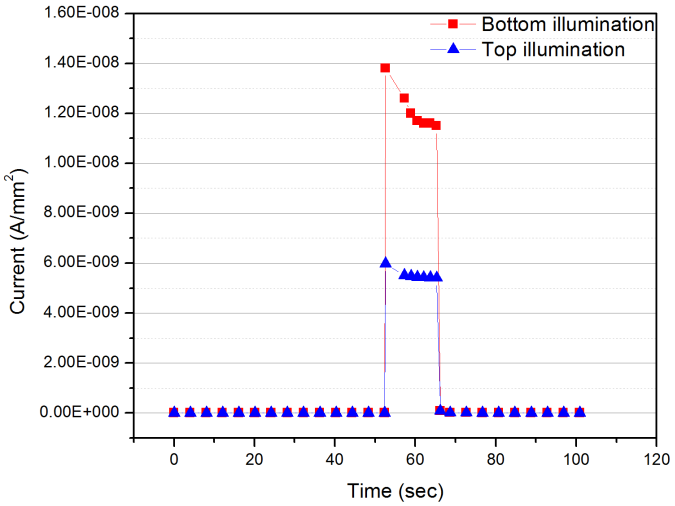

Figure 4.23: Top and bottom illumination response at 120V ($12V/\mu m$) - Green light at intensity of $10\mu W/cm^2$ (spacing and width of $10\mu m$)

and bottom illumination, respectively. In top illumination case we should also consider that 10 percent of incoming light is absorbed in PI layer. Hence, IQE of the device with spacing and width of $10\mu m$ at 120V for top and bottom illumination is 24 and 35 percent, respectively. This implies the fact that although the electric field below the electrodes is lower than within electrodes, still collection occurs there. This is because we are able to operate device at such a high field (up to $15V/\mu m$). On the other hand, since linear behaviour regarding incident power is observed, we can conclude that no photo-gain is happening and the reason for achieving an IQE higher than fill factor is the collection below the electrodes which has not observed before in lateral a-Si MSM-PD [56, 16, 8]

4.3.7 Wavelength Dependence

The indirect detection technique requires a phosphor layer to convert X-ray to visible light. In this type of detection the total conversion gain is a product of the phosphor conversion efficiency and the effective quantum efficiency of the detector. Hence in order to achieve maximum efficiency, the peak of the emission spectrum of the phosphor layer should match the absorption spectra of the detector. Gd2O2S:Tb and CsI:Tl are the most commonly used phosphors in flat-panel imagers [ref: karim's course note]. Table 4.1 indicates different types of phosphors and their properties. As it is shown, the maximum conversion gain happens around $\lambda = 550nm$ for CsI:Tl. On the other hand, in a conventional digital radiography system, p-i-n photodiodes are used which have shown low quantum efficiency at low wavelength due to absorption of blue light in the p layer [2]. In our proposed structure, a wide spectrum response is expected since there is no p doped layer within the structure. Dependence of the detector responsivity to wavelength is shown in figure 4.24 . Maximum efficiency happens in the green region ($\lambda = 525nm$) which matches maximum emissions of scintillator to achieve highest conversion gain. At lower wavelength, responsivity decays due to absorption of photons near the glass/amorphous silicon interface which leads to lower collection efficiency (lower electrical field at the glass/a-Si interface than bulk a-Si). However, the response of the proposed photodetector at short wavelength is better than conventional p-i-n photodiodes.

Table 4.1: Physical properties of inorganic phosphors

Type	Z	K-edge energy (keV)	Maximum emission wavelength (nm)	Conversion gain Γ (keV^{-1})
CaWO4	74	69.5	480±100	30
Gd2O2S:Tb	64	50.2	550±20	60
CsI:Na	55/53	36/33	415±50	40
CsI:Tl	55/53	36/33	560±80	55

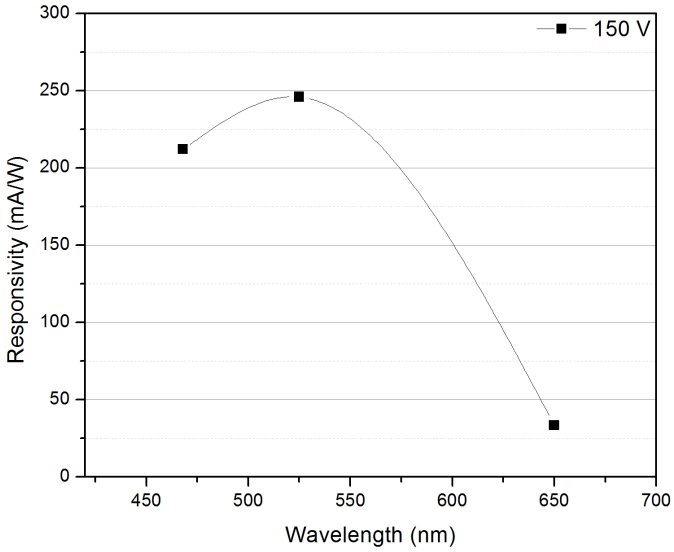

Figure 4.24: Responsitivity for three different wavelength. Device: a-Si MSM-PD with thin PI and width and spacing of $10\mu m$. Intensity: $18\mu W/cm^2$.

4.3.8 Temporal Response

In addition to dark current and responsivity, temporal response is an important metric especially for applications such high projection rate CT and fluoroscopy. Response speed is determined by minority carrier lifetime and mobility. When illumination terminates, due to the low mobility of electrons in a-Si (in compare to c-Si) and shorter motion path, chance of recombination of photogenerated electrons with holes is low, consequently, photogenerated carrier will last longer. Hence, carriers having longer life time which leads to lower speed. One way to improve transient response in the lateral MSM photodetector is reducing electrode spacing. However, reducing the spacing in comb structure leads to higher dark current and reduced fill factor. The measurement set-up used is described in chapter 3. Figure 4.25 demonstrates the transient response of a-Si MSM-PD (width and spacing of $10\mu m$) to blue light at intensity of $18\mu W/cm^2$ with "on" and "off" period of $5msec$. Therefore, fall time and rise time of around $1msec$ is achievable, which is 3 times higher than previously reported a-Si photodetector [57, 58, 59]. This is primarily due to operating the device in such a high voltage.

Overall, lateral amorphous silicon MSM photodetector with polymer blocking layer (polyimide) demonstrates great performance in terms of dark current, dynamic range and external quantum efficiency. It should be noted that by utilizing an anti-reflective layer, a quantum efficiency of 85 percent is also achievable. In order to reach a quantum efficiency more than 85 percent and faster detector, a vertical MSM structure is recommended due to the uniform electric field distribution through out the bulk of the active layer. However, there are some challenges attributed to fabrication of the vertical structure which are covered in following chapter.

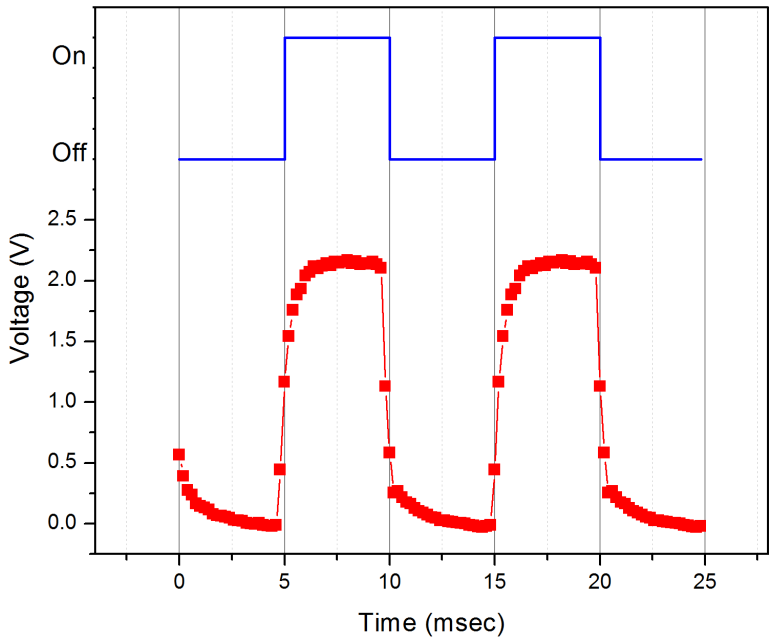

Figure 4.25: Temporal response of lateral a-Si MSM-PD to pulse light width of $5msec$ and period of $10msec$. Device is biased at $120V$ with width and spacing of $10\mu m$. Light source: Blue - Intensity: $18\mu W/cm^2$.

Chapter 5

Vertical a-Si MSM Photodetector

Hitherto, we have discussed the performance of a lateral a-Si MSM photodetector and demonstrated improvements by introducing a thin blocking layer (polyimide) between amorphous silicon and the metal contacts. Advantages which are attributed to lateral MSM photodetectors have been named including low cost and simple fabrication process, compatibility with TFT fabrication process, no top electrode to block incoming photons, low dark current, high quantum efficiency and *etc.*. In order to achieve high transient response (fall and rise time less than $1ms$), shrinking electrode spacing in the lateral structure is one way to be considered. However, shrinking electrode spacing leads to higher dark current and consequently reduces operating voltage of the detector, losing quantum efficiency. Therefore, in order to have the ability to operate the detector at high frame rates and obtain quantum efficiency greater than 85 percent, using vertical structure is suggested primarily due to uniform electric field through out the bulk of a-Si as well as shorter spacing between electrodes. However, there are some challenges attributed to the vertical structure that need more investigation to overcome. In this chapter, first perfor-

mance of fabricated vertical MSM photodetector is demonstrated in terms of dark current and response, followed by challenges which need more investigation to obtain desirable performance.

5.1 Device Structure

Since the lateral a-Si MSM structures exhibit remarkable performance in dark current and responsivity by utilizing a blocking layer, the same structure was applied to the vertical MSM. Figure 5.1 shows vertical structure. Two types of Indium Tin Oxide coated glass (ITO) have been used as a bottom transparent electrode, including textured and smooth surface. Textured surface improves responsivity of the detector due to inhibiting photons from escaping layers. However, it has been understood that a textured substrate increases dark current. Polyimide on both sides has been spin coated in the same way that it has been done on the lateral structure. Regarding amorphous silicon, due to limitations on Plasma Enhanced Chemical Vapour Deposition (PECVD) machine, we weren't able to deposit the i-layer with the same machine and recipe that we did for the lateral structure. In the PECVD machine that was used for lateral structure, the substrate faces down inside the chamber. In the vertical structure, unlike lateral, for a-Si deposition, ITO glass is coated with the polyimide layer which is facing down in the chamber of the PECVD machine with a deposition temperature of $260C$, therefore there is a risk of polyimide delaminatingis high. in courtesy of other lab users and to avoid contamination, I switched to different machine (Plasmatherm system). Also, Aluminium was used for top electrode.

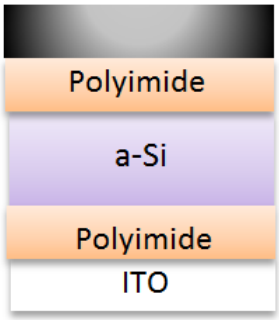

Figure 5.1: Cross section of vertical structure.

5.2 Dark and Photoresponse

As it was mentioned in earlier chapters, dark current in metal-semiconductor-metal photodetectors stems from two mechanisms including thermal generation (dominant at low electric field) and quantum mechanic tunnelling through the barrier of metal/semiconductor interface (dominant at medium and high electric field). Introducing the polyimide layer as a blocking layer prevents tunnelling of charge carriers and consequently lowers dark current. In a previous chapter we demonstrated that this idea works for the lateral structure. However, as it is shown in figure 5.2 , dark current in the vertical structure is increasing dramatically with voltage which suggests the fact that tunnelling is occuring. The dark current issue limits the device to operating at low voltage biases (low electric field). As it is mentioned before, in order to achieve high collection efficiency and conduction in polyimide in light mode, voltage across polyimide must provide at least a $1.4MV/cm^2$ electric field inside polyimide layer [conduction-PI]. Hence, high dark current leads to lower photoresponse as shown in figure 5.3 . This photoresponse yields external quantum efficiency of around 5 percent.

One possible reason that results in poor performance of the vertical MSM structure,

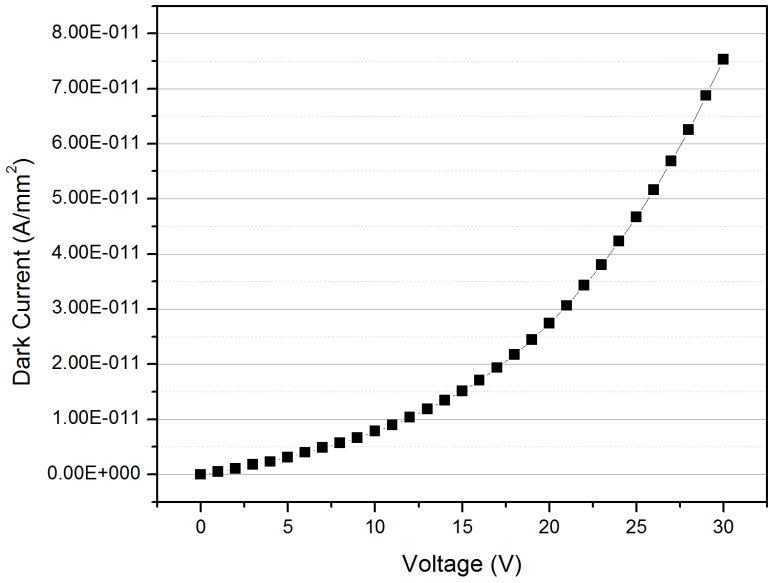

Figure 5.2: Dark current as a function of voltage in vertical MSM photodetector.

might be a non-perfect polyimide/amorphous silicon interface due to exposure of polyimide to plasma in the PECVD system. In order to avoid this issue, we can introduce a very thin passivation layer in between polyimide and amorphous silicon, optimize the amorphous silicon recipe to improve the PI/a-Si interface or find an alternative for polyimide like polystyrene. More investigation is needed to improve the performance of the vertical a-Si MSM photodetector.

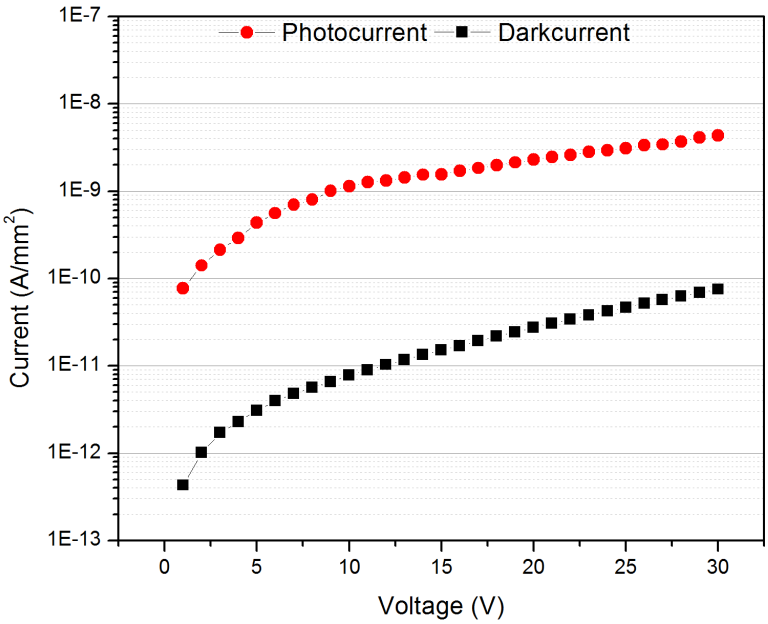

Figure 5.3: Dark and photoresponse of vertical MSM structure. Light source: Green $\lambda = 525nm$ at intensity of $80\mu W/cm^2$.

Chapter 6

Conclusion

The most promising technology for radiography is active matrix flat panel imaging systems (AMFPI). However, AMFPI systems are relatively expensive in comparison with conventional computed radiography (CR) systems. Therefore for general radiography applications low cost systems are needed, especially in hospitals and healthcare systems of the developing countries. The focus of this research is the fabrication and characterization of a low cost amorphous silicon metal-semiconductor-metal photodetector as a photosensitive element in a AMFPI systems. Here the criteria considered for the MSM-PD are performance quality and potential to be manufacturable as a low cost digital radiography system. AMFPI technology is the same as a-Si:H TFT manufacturing technology used to make display. Photosensitive element in AMFPI is a part that increases the cost of the flat panel imager. Currently most of AMFPIs benefit from the p-i-n photodiodes. However, due to the necessity of doped p^+ layer, fabrication of photodiode cannot be performed with the same process as a-Si:H TFT. In this work a new lateral a-Si MSM-PD structure is proposed as a replacement for p-i-n photodiode which is commercially used in flat panel

imager.

Metal-Semiconductor-Metal photodetectors (MSM-PD) are attractive as sensors due to their ease of fabrication and compatibility with thin film transistor fabrication process primarily because there is no p^+ doped layer in comparison with conventional p-i-n photodiodes. Previously reported a-Si MSM-PDs exhibited high dark current, instability of dark current and lower EQE in compared to the conventional p-i-n photodiodes. The main challenge in this research was finding an approach to minimize and stabilize dark current without any significant deterioration in its performance through systematic studies on photoresponse of the detector. We have demonstrated low dark current a-Si MSM-PD (lower than $20pA/mm^2$) with responsivity of $280mA/W$ and EQE of 65 percent to green light ($\lambda = 525nm$). These improvement are achieved by introduction of a PI blocking layer and operating the device at high electric field ($15V/\mu m$). This new structure eliminates the need of p^+ and n^+ layers which makes this structure fully compatible with the a-Si:H TFT fabrication process and consequently a low cost flat panel imager.

Dark current in the a-Si MSM-PD origins from thermal generation and quantum mechanical tunnelling (thermionic emission) of carriers through the metal/a-Si barrier. Instability of dark current in previously reported a-Si MSM-PDs stems from the variation of the barrier width at the metal/a-Si interface overtime. This leads to variation of tunnelling rate and consequently instability of dark current. Introducing PI blocking layer reduces the tunnelling rate and maintain dark current in the range of the thermal generation of a-Si. Hence, variation of the barrier width at the metal/a-Si interface does not affect dark current in a-Si MSM-PD with PI blocking layer. In addition to dark current and responsivity, we have studied the behaviour of the detector to the flux of the incident photons. Linear behaviour is expected in all range of the photon flux. However, at high intensity sub-linear behaviour is observed. We demonstrated that since the detector main-

tains its linear behaviour better at higher electric field ($15V/\mu m$) than lower electric field ($10V/\mu m$), the mechanism that attributed to the sub-linear behaviour at high intensity is the dependence of the mobility life-time product to the number of incoming photons. Moreover, we presented a wide detection dynamic range from $200nW/cm^2 - 300\mu W/cm^2$ with linear responsivity.

Further, in order to find the best configuration of the lateral structure, we have studied the effect of the spacing and width of the comb structure. Based on the electric field simulation in the lateral structure and the non-uniform electric field distribution, although absorption occurs below the electrodes (bottom illumination case), lower collection efficiency is expected there. Hence, higher fill factor is favourable to have higher quantum efficiency. However, due to the shape of the electric field distribution in PI layer at the edge of the Al/PI interface, shrinking the width of the electrode will result in higher dark current (even at the same voltage and spacing) and consequently confines the detector to operated at lower bias voltage which results in lower EQE. Based on experimental results, lateral structure with spacing and width of $15\mu m$ and $10\mu m$ (fill factor of 60 percent) demonstrated the best performance at 210 V bias voltage. Moreover, for the first time we experimentally showed that although the electric field below the electrodes is lower than within the electrodes in bulk of the a-Si, collection occurs below the electrodes (but with lower efficiency). This implies that even with fill factor of 60 percent, EQE more than 60 is achievable. We also present the response spectrum of the detector which shows wider spectrum than p-i-n photodiodes especially in lower wavelength (blue region) due to eliminating p^+ layer. Finally, we demonstrated rise and fall time of $1msec$ which is three times lower than previously reported a-Si MSM-PD which can be attributed to operating the detector at high electrical filed and having higher collection efficiency.

References

[1] F. H. Attix. *Introduction to Radiological Physics and Radiation Dosimetry.* John Wiley, New York, 1986.

[2] R. A. Street. *Hydrogenated Amorphus Silicon.* Cambridge University, London, 1991.

[3] Mohammad Hadi Izadi. *Multi-mode Pixel Architectures for Large Area Real-Time X-ray Imaging.* PhD thesis, University of Waterloo, 2010.

[4] Siebert JA. Digital radiography: the bottom line comparison of cr and dr technology. *Appl Radiol*, 2009.

[5] Michael Musashi Adachi. *Development and characterization of PECVD grown silicon nanowires for thin film photovoltaics.* PhD thesis, University of Waterloo, 2012.

[6] Koorosh Aflatooni. *X-Ray Detection Using Amorphous Silicon Technology.* PhD thesis, University of Waterloo, 1998.

[7] H. Scher and E. W. Montroll. Anomalous transit-the dispertion in amorphous solids. *Phys. Rev. B*, 1975.

[8] F. Taghibakhsh, I. Khodami, and K. S. Karim. Characterization of short-wavelength-selective a-si:h msm photoconductors for large-area digital-imaging applications. *IEEE Trans Electron Devices*, 2008.

[9] K. Aflatooni, R. Homsey, and A. Nathan. Reverse current instabilities in amorphous silicon schottky diodes: Modeling and experiments. *IEEE Trans. Electron Devices*, 1999.

[10] Kevles and Bettyann Holtzmann. *Naked to the Bone Medical Imaging in the Twentieth Century*. Camden, NJ, 1996.

[11] Sample Sharro. The electromagnetic spectrum., x-rays. Technical report, NASA, 2007.

[12] W.R. Hendee and E.R. Ritenour. *Medical Imaging Physics*. Wiley-Liss, NY, 2002.

[13] S. Abbaszadeh, N. Allec, S. Ghanbarzadeh, U. Shafique, and K. S. Karim. Investigation of hole-blocking contact for high conversion gain amorphous selenium detectors for x-ray imaging. *IEEE Trans Electron Devices*, 2012.

[14] M.J. Yaffe and J.A. Rowlands. X-ray detectors for digital radiology. *Physics in Medicine and Biology*, 1997.

[15] M. Bath, P. Sund, and L.G. Mansson. Evaluation of the imaging properties of two generations of a ccd-based system for digital chest radiography. *Medical Physics*, 2002.

[16] F. Taghibakhsh and K. S. Karim. Fabrication and characterization of nickel amorphous silicon metalsemiconductormetal photoconductors. *Proc. 20th Can. Conf. Elect. Comput. Eng.*, 2007.

[17] C. Kittel. *Introduction to Solid State Physics*. John Wiley and Sons, New York, 1986.

[18] A. Madan and M.P. Shaw. *The Physics and Applications of Amorphous Semiconductors*. Academic Press, 1988.

[19] Z. E.Smith and S. Wagner. Implications of the defect pool concept for metastable and stable defects in amorphous silicon. *Amorphous Silicon and Related Materials. World Scientific*, 1989.

[20] D.L. Staebler and C.R. Wronski. Reversible conductivity changes in dischargeproduced amorphous si. *Appl. Phys. Lett*, 1977.

[21] A. Shah, P. Torres, R. Tscharner, N. Wyrsch, and H. Keppner. Photovoltaic technology: The case for thin-film solar cells. *Science*, 1999.

[22] J. Meier, R. Fluckiger, H. Keppner, and A. Shah. Complete microcrystalline p-i-n solar cell crystalline or amorphous cell behavior? *Appl. Phys. Lett*, 1994.

[23] D. L. Rogers. Integrated optical receivers using msm detectors. *J. Lightwave Technol.*, 1991.

[24] S. M. SZE, D. J. COLEMAN, and A. LOYA. Current transport in metal-semiconductor-metal (msm) structures. *Solid-Stare EIecfronics*, 1971.

[25] C. W. Slayman and L. Figueroa. Frequency and pulse response of a novel high speed interdigital surface photoconductor (idpc). *IEEE Electron Dev. Lett.*, 1981.

[26] L. Figueroa and C. W. Slayman. A novel heterostructure interdigital photodetector (hip) with picosecond optical response. *IEEE Electron Dev. Lett.*, 1981.

[27] C. J. Wei, H. J. Klein, and H. Beneking. Symmetrical mott barrier as a fast photodetector. *Electron Lett*, 1981.

[28] U. Schade, S. Kollakowski, E. H. Bottcher, and D. Bimberg. Improved performance of large-area inp/ingaas metal-semiconductor-metal photodetectors by sulfured passivation. *Appl. Phys. Lett*, 1994.

[29] S. D. Kwon, C. H. Kim, H. K. Kwon, B. D. Choe, and H. J. Lim. Interface properties of (nh4)2sx-treated in0.5ga0.5p schottky contacts. *J. Appl. Phys.*, 1995.

[30] C. R. Moon, B. D. Choe, S. D. Kwon, and H. Lim. Difference of interface trap passivation in schottky contacts formed on (nh4)2sx-treated gaas and in0.5ga0.5p. *J. Appl. Phys.*, 1997.

[31] W. C. Koscielniak, R. M. Kolbas, , and M. A. Littlejohn. Photocurrent enhancement in a gaas metal-semiconductor-metal photodetector due to ultrasmall au islands. *Appl. Phys. Lett.*, 1988.

[32] P. Ambree and K. Wandel. Plasma enhanced chemical vapor deposited sio2 layers for passivation of ingaas:fe metal-semiconductor-metal photodetectors. *J. Appl. Phys.*, 1995.

[33] S. Kollakowski, U. Schade, E. H. Bottcher, D. Bimberg D. Kuhl, P. Ambree, and K. Wandel. Silicon dioxide passivation of inp/ingaas metal-semiconductormetal photodetectors. *J. Vac. Sci. Technol.*, 1996.

[34] M. A. Martin and J. G. Simmons. Polyimide passivated semitransparent in0.49ga0.51p/gaas msm photodetector operating at 840 nm wavelength. *Microwave and Optical Technol. Lett.*, 1999.

[35] L. F. Lester, K. C. Hwang, J. Mazurowski P. Ho, J. M. Ballingall, J. Sutliff, J. Whitaker S. Gupta, and S. L. Williamson. Ultrafast long-wavelength photodetectors fabricated on low-temperature ingaas on gaas. *IEEE Photon. Technol. Lett.*, 1993.

[36] S. Y. Chou, Y. Liu, , and P. B. Fischer. Fabrication of sub-50 nm finger spacing and width high-speed metal-semiconductor-metal photodetectors using highresolution electron beam lithography and molecular beam epitaxy. *J. Vacc. Sci. Technol.*, 1992.

[37] J. Y. L. Ho and K. S. Wong. Bandwidth enhancement in silicon metalsemiconductor-metal photodetector by trench formation. *IEEE Photon. Technol. Lett.*, 1996.

[38] J. Y. L. Ho and K. S. Wong. High-speed and high-sensitivity silicon-on-insulator metal-semiconductor-metal photodetector with trench structure. *Appl. Phys. Lett.*, 1996.

[39] L. H. Laih, T. C. Chang, Y. A. Chen, W. C. Tsay, and J. W. Hong. Characteristics of msm photodetectors with trench electrodes on p-type si wafer. *IEEE Trans. Electron Dev.*, 1998.

[40] L. H. Laih, T. C. Chang, Y. A. Chen, W. C. Tsay, and J. W. Hong. A u-grooved metal-semiconductor-metal photodetector (ymsm-pd) with an i-a-si:h overlayer on a [100] p-type si wafer. *IEEE Photon. Technol. Lett.*, 1998.

[41] C. S. Lin, R. H. Yeh, C. H. Liao, , and J. W. Hong. Improving characteristics of sisawed trench-electrode metal-semiconductor-metal photodetectors using self-aligned process. *IEEE Proc.-Optoelectron.*, 2001.

[42] Mohammad R. Esmaeili-Rad and Sayeef Salahuddin. High performance molybdenum disulfide amorphous silicon heterojunction photodetector. *Sci. Rep*, 2013.

[43] N. Kramer and C. V. Berkel. Reverse current mechanisms in amorphous silicon diodes. *Appl. Phys. Lett*, 1994.

[44] R A. Street. Long-time transient conduction in a-si:h p-i-n devices. *Phil. Mag. B*, 1991.

[45] J. K. Aron and S. J. Fonash. Origins of reverse bias leakage current in hydrogenated amorphous silicon p-i-n detector structures. *Appl. Phys. Lett.*, 1992.

[46] J. K. Aron and S. J. Fonash. Using reverse bias currents to differentiate between bulk degradation and interfacial degradation in hydrogenated amorphous silicon p-i-n structures. *J. Appl. Phys.*, 1992.

[47] R. Homsey, K. Aflatooni, and A. Nathan. Reverse current transient behaviour in amorphous silicon schottky diodes at low biases. *Appl. Phys. lett.*, 1997.

[48] T. Tiedje and A. Rose. A physical interpretation of dispresive transport in disordered semiconductors. *Solid state communications*, 1980.

[49] C. R. Wronski and D. E. Carison. Surface states and barrier heights of metal-amorphous silicon schottky barriers. *Solid State Comm.*, 1977.

[50] Anthony W. Sarto and Bart J. Van Zeghbroeck. Photocurrents in a metalsemiconductormetal photodetector. *IEEE JOURNAL OF QUANTUM ELECTRONICS*, 1997.

[51] J. I. Ruy, S. H. Won, J. H. Hur, H. J. Kim, and J. Jang. Simulation of a novel amorphous silicon photoconductor array. *J. Korean Phys. Soc.*, 2001.

[52] R. E. Stearns and R. L. Weisfield. Two dimensional amorphous-silicon photoconductor array for optical imaging. *J. Appl. Opt.*, 1992.

[53] Masanori Ito and Osamu Wada. Low dark current gaas metal-semiconductor-metal(msm) photodiodes using wsix contacts. *IEEE JOURNAL OF QUANTUM ELECTRONICS*, 1986.

[54] Yu Chin Lim and Robert A. Moore. Properties of alternately charged coplanar parallel strips by conformal mappings. *IEEE TRANSACTIONS ON ELECTRON DEVICES,*, 1968.

[55] N. R. Tu and K. C. Kao. High-field electrical conduction in polyimide films. *J. Appl. Phys*, 1999.

[56] S. Abbaszadeh, N. Allec, and K.S. Karim. Characterization of low dark-current lateral amorphous-selenium metal-semiconductor-metal photodetectors. *Sensors Journal, IEEE*, 2013.

[57] J. H Siewerdsen and D. A. Jaffray. A ghost story: Spatio-temporal response characteristics of an indirect-detection flat-panel imager. *Med. Phys.*, 1999.

[58] S. Takayama, K. Mori, K. Suzuki, and C. Tanuma. An a-si:h photoconductive sensor with a gate electrode. *IEEE Trans. Electron Devices*, 1993.

[59] J. A Seibert. Flat-panel detectors: how much better are they? *Pediatr Radiol*, 2006.